J. CHEM. SOC. FARADAY TRANS., 1995, 91(19), 3415–3432

Stresses in Lipid Membranes and Interactions between Inclusions

Peter A. Kralchevsky,* Vesselin N. Paunov and Nikolai D. Denkov
Laboratory of Thermodynamics and Physico-chemical Hydrodynamics, University of Sofia, Faculty of Chemistry, Sofia 1126, Bulgaria
Kuniaki Nagayama
Protein Array Project, ERATO, JRDC; 5-9-1 Tokodai, Tsukuba 300-26, Japan

This study is devoted to a theoretical model of the membrane-mediated interactions between inclusions (proteins) incorporated into lipid bilayers. The interactions are due to the overlap of the bilayer deformations around each of two approaching inclusions. To determine the resulting stresses in the membrane we have developed an appropriate model of the lipid bilayer, which has been described as an elastic layer (the hydrocarbon-chain region) sandwiched between two Gibbs dividing surfaces (the two headgroup regions). Expressions for the membrane stretching and bending elastic moduli have been derived in terms of the lipid monolayer tension and elastic constants. The interaction between two cylindrical inclusions have been calculated by using both force and energy approaches. The range of this interaction turns out to be of the order of several inclusion radii. The results, which are in qualitative agreement with the experimental observations, can be applied to the interpretation of membrane processes and mechanisms, such as protein aggregation in lipid membranes, as well as to any process affected by the membrane stretching and bending elastic properties.

It has been experimentally established that some integral proteins may aggregate in native membranes to form two-dimensional crystals.[1–5] Two well known examples are the bacteriorhodopsin in the membranes of *Halobacterium halobium*[1,2] and the connexons in the communicating cells.[3,4] On the other hand, many proteins are known to function in a non-aggregate state. Thus, the rhodopsin from retinal-rod membranes changes its properties significantly upon aggregation and immobilisation.[6] It is widely accepted that the lateral heterogeneity of membrane proteins plays an important role in biological phenomena such as endocytosis,[7] immunoresponses and the processes of patching and capping,[8] enzymatic reactions[8,9] and intercellular interactions.[7] The different types of forces leading to protein aggregation or disaggregation in the membranes are a matter for extensive studies, both experimental and theoretical.

A particular type of non-specific interaction between integral proteins is mediated by their lipid environment (the so-called 'lipid-mediated interaction'[10–12]). The main idea for such an interaction comes from the experimental observations that the proteins perturb the neighbouring lipid molecules.[8,13–21] Theoretical models have been developed by Marcelja,[10] Schröder,[11] and Owicki *et al.*[22,23] The experiments with electron paramagnetic resonance (EPR) techniques showed that two distinct signals can be detected in natural membranes or artificially constructed lipid bilayers containing a given type of integral protein. The EPR spectrum was explained with the presence of two different populations of lipids: (i) the signal corresponding to hindered motion of lipid molecules was attributed to lipids tightly bound to the protein, (ii) the other signal, which was equivalent to that for the membrane without incorporated proteins, was attributed to the remaining lipid molecules which were not in contact with the protein.[14,16,17] From the concentration dependence of the spectrum it was determined that about one layer of lipids is immobilised around each of the protein molecules.[14,20,21] The later experiments performed by means of EPR and NMR methods specified the complex picture of the protein–lipid interaction. It was shown that the exchange rate of the lipids in contact with the protein is about one order of magnitude lower than that for free lipids in the fluid lipid bilayer.[21] Nevertheless, the experiments demonstrated that the degree of ordering and fluidity of the hydrocarbon chains of the bound molecules are not very different from those for the free molecules (in contrast with the initial hypotheses[10,11]), see ref. 8, 13, 15. The absence of considerable ordering of the lipid tails was explained[8] by the irregular shape of the protein molecules (the protein structure is more rigid and the lipid tails should follow the shape of the outer protein surface). The decreased rate of lipid exchange was attributed to non-specific (mainly electrostatic) interactions between the headgroups of the lipid molecules and the proteins.[15,20] In some cases the immobilisation of the lipid molecules was explained by them being captured in the space between aggregated protein molecules.[8,15,16] In general, the recent experimental studies show that in many cases the ordering parameter of the lipids in close vicinity of a protein molecule is close to that for the free molecules.[15,24,25] This finding does not favour the theoretical models developed in ref. 10, 11, 22 and 23.

Chen and Hubbell[26] found experimentally that the transmembrane protein rhodopsin was dispersed when in bilayers made with di-10 : 0 phosphatidylcholine, while it was aggregated in di-18 : 1 *trans*-phosphatidylcholine bilayers. The configurations of the proteins in the former and latter bilayers resemble those depicted in Fig. 1(a) and (b), respectively. One can conclude that the perturbation of the bilayer thickness caused by the protein can lead to protein–protein attraction. Note that the width of the protein hydrophobic belt can be both smaller [Fig. 1(b)] and greater [Fig. 1(c)] than the hydrophobic thickness of the non-perturbed bilayer.

Israelachvili[12] discussed possible origins of the lateral protein–protein interaction. In particular, he proposed a possible source for the interaction between two different membrane proteins, with hydrophobic belts thinner and thicker than the bilayer hydrophobic thickness, the so-called 'mismatch'; Fig. 1(d). He anticipated that this interaction could be repulsive, analogous to that between two floating bodies in water, which depends on the shapes of the menisci in a vicinity of the bodies. Note that the mechanism proposed by Marcelja[10] does not presume formation of menisci; see Fig. 1(a).

The effect of the mismatch of the hydrophobic regions on the aggregation behaviour of proteins has been studied both experimentally[16,19,27–29] and theoretically.[30,31] For instance, Lewis and Engelman[27] showed that bacteriorhodopsin forms

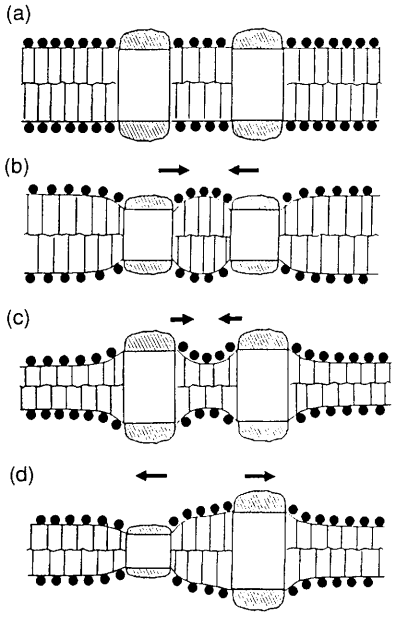

Fig. 1 Inclusions (membrane proteins) in a lipid bilayer: (a) the hydrophobic thicknesses of the bilayer and inclusions coincide; (b)–(d) the hydrophobic thicknesses of bilayer and inclusions are different: the overlap of the deformations around the inclusions lead to a lipid mediated protein–protein interaction

aggregates in vesicles (prepared from lipids of different chain lengths) only when the mismatch is greater than 0.4 nm for thicker [Fig. 1(b)] and 1 nm for thinner [Fig. 1(c)] lipid bilayers. Similar protein aggregation at considerable hydrophobic mismatch was detected with other natural proteins[16,19,28] and with artificially synthesised polypeptides.[19] It was also shown in these studies that the proteins affect the phase transition temperature of the lipid bilayer.

The theoretical consideration of the effect of the hydrophobic mismatch turns out to be very closely related to the mechanical properties of the lipid bilayers. The experiments[32–37] with vesicles from a single lipid component, or from a mixture of lipids, have allowed the determination of the elastic constants for membrane stretching and bending. It was shown that their values are interrelated and strongly dependent on the membrane thickness[36,37] and on the presence of cholesterol.[13,34,35] A variety of theoretical models have been proposed for estimation of the elastic constants.[32,38–41] Generally, one can distinguish two types of model. The first type is based on explicit modelling of the interaction between the lipid molecules (van der Waals, electrostatic, *etc.*) and on a numerical analysis of the configurational entropy of the lipid chains.[38,39] Among these models, the most useful turns out to be the mean-field class of models where the energy and entropy of a given molecule are calculated by averaging over all possible chain configurations of the neighbours.[42–44] These models are very suitable for studying the properties of homogeneous amphiphilic aggregates (micelles, microemulsions, lipid bilayers), *e.g.* for calculation of their spontaneous curvature, elastic constants or chain packing (chain-order parameter). Two important conclusions were drawn in these studies: (i) that the CH_2-group density and ordering are rather uniform across the membrane[39,43,44] and (ii) that the lipid tails strongly interact with each other and create substantial mechanical stresses.[38,39,43] This can be interpreted as an accumulation of elastic energy in the hydrocarbon-chain region, Fig. 2. However, at present, this type of theory is hard to apply for investigating complex processes such as lipid-mediated protein interactions. From this viewpoint the second type of

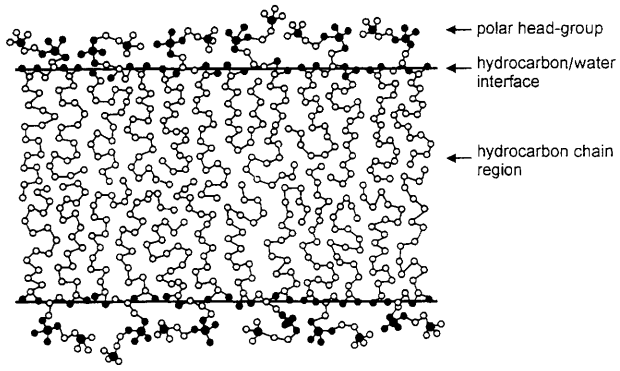

Fig. 2 Lipid (lecithin) bilayer drawn to scale (after ref. 57)

phenomenological models are more versatile.[25,32,38,40,41] In this approach the energy variation around a given (non-perturbed) state is calculated by using some phenomenological parameters (Young's modulus, interfacial tension, and others) which can be experimentally measured or calculated from microscopic (molecular) considerations. Some of these models account only for the elasticity of the hydrophobic core of the lipid bilayer,[32,40] while other models also consider the interfacial energy at the boundary with the adjacent aqueous phases.[25,32,38,41]

Helfrich and Jakobsson[45] calculated the energy of formation of a concave or convex meniscus around an integral membrane protein (gramicidin channel). They determined the meniscus shape by using a modified version of Huang's[46] equation, which takes into account contributions due to the bending elasticity, surface tension and the normal compressibility of the bilayer. These authors considered quantitatively both solvent-free and solvent-containing (swollen) membranes. On the other hand, their theoretical analysis was restricted to the meniscus on a single protein and did not treat the protein–protein interaction. The latter was studied theoretically by Dan *et al.*[47] on the basis of a postulated model expression for the free energy per molecule of a curved monolayer (as a constituent part of the bilayer). The results obtained by these authors depend to a great extent on the adequacy of the model expression postulated by them (see discussion below).

Here we propose an alternative theoretical approach to the membrane-mediated interactions between inclusions, which is based on a recent advance in the theory of lateral capillary forces.[48–50] A first step in this direction was made in ref. 51 where the protein–protein interaction in a membrane was treated in a similar manner to the interaction between two colloidal particles which are partially immersed in a thin liquid film. However, to describe protein–protein interactions adequately in biomembranes the approach of ref. 51 requires a generalisation, at least in two directions:

(1) Solvent-free membrane should be considered and the elasticity of the hydrocarbon-chain region should be accounted for (note that the approach in ref. 51 is appropriate for a solvent-containing membrane).

(2) Bending-moment and bending-elasticity effects should be taken into account along with the surface-tension effect.

The aim of the present study is to provide a generalised and quantitative theory of capillary meniscus interactions between membrane proteins incorporated in a lipid bilayer. In the present article we consider proteins (inclusions) of cylindrical shape like those depicted in Fig. 1. In this case the deformation consists of a variation of the bilayer thickness, whereas the bilayer midplane remains planar [Fig. 1(b)–(d)]. Such a mode of deformation corresponds to the squeezing mode observed with thin liquid films.[52,53]

In Appendix A we consider the supplementary bending mode of bilayer deformation, which consists of bending of the midsurface at constant film thickness. The calculated bending elastic moduli can be important for the quantitative description of the long-range membrane-induced interactions resulting from perturbations of the bilayers long-wavelength shape fluctuations; the latter effect has been determined theoretically by Goulian *et al.*[54]

The key for solving the aforementioned problems is the formulation of a realistic and adequate rheological model of the bilayer membrane. It is generally accepted that a lipid bilayer behaves as a two-dimensional fluid at body temperature. This fact is taken into account in the two-dimensional hydrodynamics of motion of inclusions throughout a membrane.[55] On the other hand, the bilayer exhibits elastic properties in processes accompanied by extension or compression of the hydrocarbon chains of the lipids. Such a process can be an uniform stretching or squeezing mode of deformation [Fig. 1(b)–(d)]. The situation becomes more complicated because it is not always appropriate to model the bilayer interior (Fig. 2) as an isotropic elastic body.[32,38]

In summary, a bilayer can exhibit different rheological behaviour (*viz.* fluid, elastic or hybrid behaviours) depending on the mode of deformation. This is not surprising because a bilayer is neither a three-dimensional nor a two-dimensional continuum; and the hydrocarbon-chain region (Fig. 2) is neither an isotropic liquid nor a solid. A natural approach to the mechanics of such a complex body is to use different constitutive relations (connecting stress and strain) for the different independent modes of deformation. For example, in the case of two-dimensional convective flow the bilayer can be treated as a two-dimensional viscous fluid.[55] As demonstrated below, the hydrocarbon-chain region can be modelled as an isotropic elastic body when the deformation modes represent bending or uniform lateral stretching. Moreover, below we propose a hybrid rheological model for the case of non-uniform lateral stretching [Fig. 1(b)–(d)]. However, for all modes of deformation we use the same 'sandwich' model of the bilayer structure, *viz.* a three-dimensional body of specified rheological behaviour (the hydrocarbon-chain region) sandwiched between two Gibbs dividing surfaces modelling the two headgroup regions, Fig. 2.

First we consider a deformation of a uniform lateral stretching, introduce the 'sandwich' model and then determine the coefficient of shear elasticity of the bilayer interior. Next we consider non-uniform lateral stretching and derive the equations governing the bilayer shape. Then we calculate the deformation created by a single inclusion and by two inclusions. Finally, we calculate the lateral force between two inclusions like those depicted in Fig. 1(b)–(d). The bending mode of bilayer deformation is examined in Appendix A and expressions for the curvature elastic moduli are derived. For the readers' convenience a list of notation has been provided.

Uniform Stretching of Bilayers

Derjaguin and Obuhov[56] proposed a generally accepted approach which treats a thin liquid film as two Gibbs dividing surfaces, whose interaction is accounted for by an excess disjoining pressure (surface force per unit area).[57,58] Here we extend this approach to lipid bilayers. The main new part of the model is that we treat the hydrocarbon interior of the bilayer as an elastic medium (rather than as a liquid phase) which is sandwiched between two Gibbs dividing surfaces modelling the headgroup regions. In the case of uniform stretching the bilayer cannot exhibit its two-dimensional fluidity. Indeed, the deformations of the hydrocarbon chains of all lipid molecules are similar and lateral slip between the chains of neighbouring molecules does not take place (Fig. 3). That is the reason why the bilayer hydrocarbon interior can be treated as an isotropic elastic medium as defined in ref. 59. (The dissimilar case of non-uniform deformation is considered separately in the next section.)

Initial State of the Bilayer

The reference state (the initial state of deformations such as those in Fig. 1) is a plane-parallel bilayer. This is a result of self-assembly of lipid molecules. Owing to the specific state of the hydrocarbon chains of the lipids built into a bilayer, some internal stresses exist in the chain region. In our approach they are modelled by stresses in an elastic medium. Similarly to the micromechanical approach to the interfaces and thin films,[60,61] we can write the pressure tensor in the chain region in the form

$$\boldsymbol{P} = P_T(\boldsymbol{e}_x\boldsymbol{e}_x + \boldsymbol{e}_y\boldsymbol{e}_y) + P_N\boldsymbol{e}_z\boldsymbol{e}_z \quad (1.1)$$

(see Fig. 4 for notation). As usual, the bilayer (film) surface tension, σ, is excess with respect to the tangential component of the bulk pressure tensor.[62]

$$\sigma = -\int_0^{h/2} [P_T^{real}(z) - P_T]\,dz - \int_{h/2}^{\infty} [P_T^{real}(z) - P_0]\,dz \quad (1.2)$$

where P_T^{real} denotes the real tangential component of the pressure tensor and P_0 is the pressure in the bulk of the aqueous phase. On the other hand, P_N and P_T are attributes of the model, which can be determined as follows.

The condition for force balance per unit area of the film surface reads (Fig. 4):

$$P_0 = P_N + \Pi \quad (1.3)$$

where Π is the disjoining pressure accounting for the excess molecular interactions across the film.[57,58] In the case of a

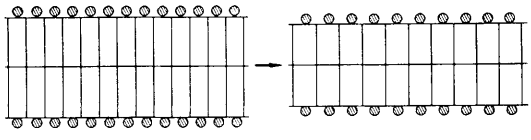

Fig. 3 Stretching of a lipid bilayer under the condition of constant volume per hydrocarbon chain

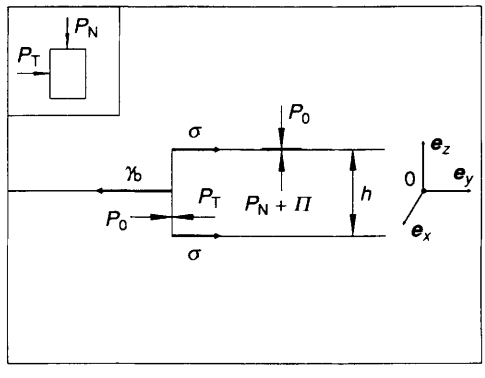

Fig. 4 Forces acting in a lipid bilayer in the reference state: γ_b is the total bilayer tension, σ is the bilayer (film) surface tension, P_0 is the pressure in the aqueous phase; Π is disjoining pressure; $\boldsymbol{e}_x$, $\boldsymbol{e}_y$ and $\boldsymbol{e}_z$ are unit vectors of the coordinate axes; P_N and P_T are the normal and tangential components of the pressure tensor exerted on an element of the elastic medium (the inset)

lipid bilayer Π originates from the van der Waals forces.[58]

$$\Pi = -\frac{A_H}{6\pi h^3} \tag{1.4}$$

where A_H is the Hamaker constant and h is the film thickness; the minus sign in eqn. (1.4) indicates attraction between the film surfaces. For a hydrocarbon film in water $A_H \approx 10^{-20}$ J (see *e.g.*, ref. 57) and with $h = 3$ nm one calculates $\Pi \approx -2 \times 10^4$ Pa. Since $P_0 \approx 10^5$ Pa (the atmospheric pressure), eqn. (1.3) shows that $P_N \approx 1.2 \times 10^5$ Pa.

The normal force balance, eqn. (1.3), can be complemented with a tangential force balance. Let γ_b be the total tension of the bilayer. From a macroscopic viewpoint γ_b characterises the bilayer as a membrane of zero thickness intervening between two aqueous phases of pressure P_0. In the framework of the detailed model depicted in Fig. 4 the stresses acting in lateral directions are characterised by σ and P_T. In view of Fig. 4 one derives

$$\gamma_b = 2\sigma + (P_0 - P_T)h \tag{1.5}$$

Eqn. (1.5) is a version of the Rusanov equation originally derived for a thin liquid film.[63] The comparison of eqn. (1.2) and (1.5) shows that γ_b does not depend on the choice of the reference state:

$$\gamma_b = -\int_{-\infty}^{+\infty} [P_T^{real}(z) - P_0]\, dz \tag{1.6}$$

On the other hand, σ and P_T depend on the choice of the reference state, but once this choice has been made all parameters have well defined values for a given physical state of the real system. Such a formulation is typical for thermodynamics of the thin liquid films.[62]

The experiments[64] with dense lipid monolayers adsorbed at the hydrocarbon/water interface show that the surface pressure does not depend on the length of the hydrocarbon chains of the lipids at any area per molecule. This implies that the quantity $\sigma + (P_0 - P_T)h/2$, *cf.* eqn. (1.5), does not depend on h. In other words, the difference $|P_0 - P_T|$ is small enough and the surface pressure of such monolayers is dominated by the interactions in the headgroup region. Then it is reasonable to define σ as the interfacial tension of a lipid monolayer on a hydrocarbon/water interface at the same temperature, composition of the aqueous phase and area per lipid molecule as for the bilayer. For example, from the experimental data in ref. 65 for 1,2-distearoyl lecithin at the heptane/water (with NaCl) interface one calculates $\sigma = 14$ mN m^{-1} for an area per molecule of 67 Å^2. As the total membrane tension of a non-extended bilayer is very low, $\gamma_b \ll \sigma$ (tension free state, see ref. 32), from eqn. (1.5) one can determine P_T:

$$P_T \approx P_0 + \frac{2\sigma}{h} \tag{1.7}$$

With $\sigma = 14$ mN m^{-1}, $h = 3$ nm and $P_0 = 10^5$ Pa then $P_T = 9.4 \times 10^6$ Pa. In accordance with the definition of σ, P_T is an excess lateral pressure in the bilayer with respect to a monolayer.

The Rusanov equation, eqn. (1.5), provides a simple interpretation of the tension-free state of the bilayer, *viz.* the surface tensions of the bilayer surfaces are exactly balanced by the excess lateral pressure in the bilayer interior, *cf.* Fig. 4.

Deformation of Stretching

Consider a stretching of the bilayer and let us denote the respective changes in P_N and P_T by ΔP_N and ΔP_T. Following the approach in Section 5 of ref. 59 for a deformation of uniform stretching, one can derive

$$\tau_{xx} = \tau_{yy} = -\Delta P_T; \qquad \tau_{zz} = -\Delta P_N \tag{1.8}$$

where τ_{ij} ($i, j = x, y, z$) are components of the stress tensor (we recall that the stress equals the negative pressure). By using eqn. (1.8), the connection between strain and stress [ref. 59, eqn. (4.8)], we obtain.

$$u_{zz} = -\frac{1}{9K_e}(\Delta P_N + 2\Delta P_T) - \frac{1}{3\lambda}(\Delta P_N - \Delta P_T) \tag{1.9}$$

$$u_{xx} = u_{yy} = -\frac{1}{9K_e}(\Delta P_N + 2\Delta P_T) + \frac{1}{6\lambda}(\Delta P_N - \Delta P_T) \tag{1.10}$$

where u_{ij} ($i, j = x, y, z$) are components of the strain tensor and K_e is the compressibility modulus and λ is the coefficient of shear elasticity. We assume that $K_e \gg \lambda$, as it could be expected for a liquid-like medium. Moreover, one can expect that $|\Delta P_T| \gg |\Delta P_N|$, see below. Then it is possible to simplify our treatment from the very beginning by neglecting the terms proportional to $1/K_e$

$$u_{xx} = u_{yy} = -\frac{1}{2}u_{zz} = \frac{1}{6\lambda}(\Delta P_N - \Delta P_T) \tag{1.11}$$

The components of the strain tensor determined by eqn. (1.11) obviously obey the incompressibility condition, $u_{xx} + u_{yy} + u_{zz} = 0$. Let us introduce the bilayer dilation per unit area:

$$\alpha = \frac{\Delta A}{A} = u_{xx} + u_{yy} \tag{1.12}$$

The relative change in the film thickness is

$$\frac{\Delta h}{h} = u_{zz} = -\alpha \tag{1.13}$$

At the last step we used the condition for incompressibility. Since the bilayer extension occurs at constant outer pressure, P_0, differentiation of eqn. (1.3) along with eqn. (1.4) and (1.13) yields

$$\Delta P_N = -\Delta\Pi = -\frac{A_H}{2\pi h^3}\frac{\Delta h}{h} = -3\Pi\alpha \tag{1.14}$$

In addition, from eqn. (1.11), (1.12) and (1.14) one obtains

$$\Delta P_T = \Delta P_N - 3\lambda\alpha = -3(\Pi + \lambda)\alpha \tag{1.15}$$

For small bilayer extensions, from eqn. (1.5) one derives in linear approximation

$$\gamma_b = \gamma_{b0} + \Delta\gamma_b = \gamma_{b0} + 2\Delta\sigma + (P_0 - P_T)\Delta h - h\Delta P_T \tag{1.16}$$

where γ_{b0} denotes the value of the total film tension in the initial state. (If the latter is a tension free state, then $\gamma_{b0} = 0$.) In linear approximation one can write

$$\Delta\sigma = E_G\alpha \tag{1.17}$$

where E_G is the Gibbs elasticity of a lipid monolayer. Finally, a substitution of eqn. (1.7), (1.13), (1.15) and (1.17) into eqn. (1.16) yields

$$\gamma_b = \gamma_{b0} + K_s\alpha \tag{1.18}$$

where

$$K_s = 2\sigma + 2E_G + 3\Pi h + 3\lambda h \tag{1.19}$$

is the stretching (elasticity) modulus of the whole bilayer. The disjoining pressure Π is to be substituted from eqn. (1.4). The first two terms in the right-hand side of eqn. (1.19) represent

properties of the two film surfaces, whereas the last two terms represent a correction accounting for the fact that the two monolayers are assembled to form a solvent-free bilayer.

Fernandez-Puente *et al.*[37] estimated that the elasticity of the chain region contributes about 20 mN m^{-1} to the total stretching modulus K_s. If we can identify this contribution with the last term in eqn. (1.19), that is $3\lambda h = 20$ mN m^{-1}, with $h = 36$ Å we calculate $\lambda \approx 2 \times 10^6$ Pa.

From the data for compressibility of liquid hydrocarbons one can estimate $K_e \approx 9 \times 10^8$ Pa. One sees that $K_e \gg \lambda$ in consonance with our assumption. Moreover, with $\lambda = 2 \times 10^6$ Pa and $\Pi = -2 \times 10^4$ Pa [see the estimate after eqn. (1.4)], and by using eqn. (1.14) and (1.15), one can verify that $|\Delta P_T| \gg |\Delta P_N|$.

Note that the shear elasticity coefficient, λ, affects not only the stretching elasticity modulus, K_s, but also the total bending and torsion (Gaussian) elasticity moduli k_t and $\bar{k}_t$ of the bilayer. Therefore, in principle λ can be determined from the measured k_t or $\bar{k}_t$. The 'sandwich' model described above also provides expressions for k_t and $\bar{k}_t$:

$$k_t = 2k_c - (\tfrac{3}{4}B_{00} + \tfrac{1}{2}B'_0)h + \tfrac{1}{2}E_G h^2 + \tfrac{1}{3}\lambda h^3 \quad (1.20)$$

$$\bar{k}_t = 2\bar{k}_c + \tfrac{1}{2}B_{00}h - \tfrac{1}{6}\lambda h^3 \quad (1.21)$$

Here k_c and $\bar{k}_c$ are the bending and torsion elastic moduli of the bilayer surfaces (to be distinguished from k_t and $\bar{k}_t$, which characterise the bilayer as a whole); $B_0 = B_{00} + B'_0\alpha + \ldots$ is the series expansion of the bending moment of the bilayer surface for small values of the relative dilation α. Eqn. (1.20) and (1.21) are derived and discussed in Appendix A.

Non-uniform stretching around Inclusions

Rheological Model

Comparison between Fig. 3 and 5 shows that the bilayer deformation around a cylindrical inclusion can be considered as a deformation of non-uniform stretching. In particular, the extension of the lipid hydrocarbon chains along the z-axis (Fig. 5) is greater for molecules situated closer to the inclusion, whereas the bilayer far from the inclusion is not disturbed. The volume occupied by the hydrocarbon chains of a separate lipid molecule (one of the many small rectangles depicted in Fig. 3 and 5) can be modelled as an isotropic elastic body. On the other hand, lateral slip between molecules (neighbouring rectangles in Fig. 5) is possible, which in turn is related to the two-dimensional fluidity of the bilayer.

Hence, modes of deformation which do not include such a lateral slip (*e.g.* two-dimensional isotropic stretching, Fig. 3, or bending mode, see Appendix A) can be described by using an elastic body constitutive relation for the bilayer interior. On the other hand, modes of deformation including lateral slip between the lipid chains (see Fig. 5) must be described by using an appropriate constitutive relation, which takes into account the two-dimensional fluidity of the bilayer. With this end in view we first note that the bilayer interior can be considered as an incompressible medium,

$$\nabla \cdot \boldsymbol{u} = 0 \quad (2.1)$$

($\boldsymbol{u}$ is the displacement vector) in so far as we deal with relatively low pressure variations.

The stress tensor component in an incompressible isotropic elastic medium reads[59]

$$\tau_{ij} = 2\lambda u_{ij} \quad (2.2)$$

where, as usual, λ is coefficient of shear elasticity,

$$u_{ij} = \frac{1}{2}\left(\frac{\partial u_j}{\partial x_i} + \frac{\partial u_i}{\partial x_j}\right) \quad (2.3)$$

and u_i ($i = x, y, z$) is a component of the displacement vector $\boldsymbol{u}$. Note that eqn. (2.3) is always valid as it is a definition of u_{ij}, whereas eqn. (2.2) is a postulated constitutive relation applicable to a body which can be treated as an incompressible isotropic elastic medium. Since eqn. (2.2) does not take into account the two-dimensional fluidity of the bilayer, below we postulate another constitutive relation. The latter should be a 'hybrid' between the constitutive relations of a fluid and of an elastic body. In particular, τ_{ij} must be isotropic in the plane xy and simultaneously, to account for the elasticity of extension of the hydrocarbon chains, along the z-axis. These requirements are satisfied by the expression

$$\tau_{ij} = -p\delta_{ij}; \quad i, j = x, y, z; \quad (i, j) \neq (z, z) \quad (2.4a)$$

$$\tau_{zz} = 2\lambda u_{zz} \quad (2.4b)$$

Here δ_{ij} is the Kronecker symbol; p has the meaning of pressure characterising the bilayer as a two-dimensional fluid; on the other hand, eqn. (2.4*b*) is an analogue of eqn. (2.2).

The condition for hydrostatic equilibrium yields[59]

$$\frac{\partial \tau_{ij}}{\partial x_i} = 0; \quad j = 1, 2, 3 \quad (2.5)$$

($x_1 = x$, $x_2 = y$, $x_3 = z$). Eqn. (2.1) and (2.5) form a set of four equations for determining the four unknown functions u_x, u_y, u_z and p. This implies that the mechanical problem based on the constitutive relation, eqn. (2.4), is correctly formulated. Below we proceed with the determination of these unknown functions.

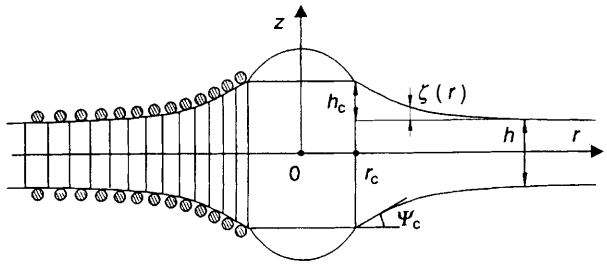

Fig. 5 Sketch of the deformation around a cylindrical inclusion of radius r_c and hydrophobic belt of width l_0; h is the thickness of the non-disturbed bilayer and h_c is the mismatch between the hydrophobic zones of the inclusion and bilayer

Deformations in the Hydrocarbon-chain Region

Eqn. (2.5) for $j = z$, along with eqn. (2.3) and (2.4*b*), yields

$$\frac{\partial^2 u_z}{\partial z^2} = 0 \quad (2.6)$$

Considerations for symmetry imply that u_z must be an odd function of z which is to satisfy the boundary condition

$$u_z|_{z=h/2} = \zeta(x, y) \quad (2.7)$$

where $z = \zeta(x, y)$ describes the shape of the upper bilayer surface. Then one obtains

$$u_z = \frac{2z}{h}\zeta(x, y) \quad (2.8)$$

The continuity eqn. (2.1) can be transformed to read

$$\nabla_{II} \cdot \boldsymbol{u}_{II} = -\frac{\partial u_z}{\partial z} \quad (2.9)$$

where $\boldsymbol{u}_{II}$ is the projection of the displacement vector $\boldsymbol{u}$ in the

plane xy and ∇_{II} is the gradient operator in the same plane:

$$\boldsymbol{u}_{II} = \boldsymbol{e}_x u_x + \boldsymbol{e}_y u_y; \qquad \nabla_{II} = \boldsymbol{e}_x \frac{\partial}{\partial x} + \boldsymbol{e}_y \frac{\partial}{\partial y} \tag{2.10}$$

We seek $\boldsymbol{u}_{II}$ in the form

$$\boldsymbol{u}_{II} = -\nabla_{II} g(x, y, z) \tag{2.11}$$

where g is an unknown scalar function. Substituting eqn. (2.8) and (2.11) into eqn. (2.9) yields

$$\nabla_{II}^2 g = \frac{2}{h}\zeta \tag{2.12}$$

In addition, the substitution of eqn. (2.4*a*) into eqn. (2.5) yields $\nabla_{II} p = 0$, hence p does not depend on x and y. Moreover, in so far as the bilayer from the inclusion(s) is not perturbed (Fig. 5) and τ_{ik} expresses a perturbation, one can conclude that p is identically zero:

$$p = 0 \tag{2.13}$$

To determine g we need a boundary condition at the inclusion surface. One can use the condition of impermeability of inclusion surface:

$$\boldsymbol{m} \cdot \boldsymbol{u}_{II} = -\frac{\partial g}{\partial m} = 0 \tag{2.14}$$

(at the inclusion surface).

Here $\boldsymbol{m}$ is a normal projecting out from the inclusion surface and $\partial g/\partial m$ is a directional derivative. The additional boundary conditions, which should be imposed at the bilayer surfaces, are considered below.

Deformation of the Bilayer Surfaces

We consider the case when the two bilayer surfaces are symmetric with respect to a planar midsurface (Fig. 5). Hence it is sufficient to describe the shape $z = \zeta(x, y)$ of the upper bilayer surface. On the other hand, we do not impose any restriction on the number of the inclusions.

Our treatment is based on the theory of liquid films of uneven thickness developed in ref. 62 and 66. The interfacial local balance of the linear momentum (for the upper bilayer surface) reads:[62,66]

$$\nabla_s \cdot \boldsymbol{\sigma} - \boldsymbol{n} \cdot (\boldsymbol{T}_I - \boldsymbol{T}_{II})|_{z=h/2} + \Pi(\boldsymbol{e}_z \cdot \boldsymbol{n})\boldsymbol{e}_z = 0 \tag{2.15}$$

where $\boldsymbol{\sigma}$ is the surface stress tensor, ∇_s is the two-dimensional gradient operator of the film surface, which is to be distinguished from the gradient operator ∇_{II} in the xy plane (the midsurface);

$$\boldsymbol{n} = (\boldsymbol{e}_z - \nabla_{II}\zeta)/(1 + |\nabla_{II}\zeta|^2)^{1/2} \tag{2.16}$$

is the unit normal out from the bilayer surface,[51]

$$\boldsymbol{T}_I = -P_N \boldsymbol{e}_z \boldsymbol{e}_z - P_T \boldsymbol{U}_{II} + \boldsymbol{\tau}; \qquad \boldsymbol{T}_{II} = -P_0 \boldsymbol{U} \tag{2.17}$$

are the stress tensors inside and outside the bilayer; $\boldsymbol{U}$ is the spacial unit tensor, $\boldsymbol{U}_{II}$ is the two-dimensional unit tensor in the plane xy; P_0 is the pressure in the aqueous phase; P_N and P_T characterise the stresses in a plane-parallel bilayer, whereas $\boldsymbol{\tau}$ as given by eqn. (2.4) takes into account the additional elastic stresses due to deformation in the bilayer (Fig. 5). Note that Π accounts for conventional surface forces,[57,58] like the van der Waals forces, whereas the elastic stresses are accounted for by $\boldsymbol{\tau}$.

Let $\boldsymbol{a}_1$ and $\boldsymbol{a}_2$ be vectors of a local basis in the bilayer surface. Then $\boldsymbol{\sigma}$ can be written in the form[61,62,67,68]

$$\boldsymbol{\sigma} = \boldsymbol{a}_\mu \boldsymbol{a}_\nu \sigma^{\mu\nu} + \boldsymbol{a}_\mu \boldsymbol{n} \sigma^{\mu(n)} \tag{2.18}$$

where $\sigma^{\mu\nu}$ and $\sigma^{\mu(n)}$ are the respective components of the surface stress tensor; the Greek indices take values 1 and 2 and summation over the repeated indices is assumed. Here and hereafter we use the formalism of the mechanics of curved interfaces; see ref. 61 for a recent review. We substitute eqn. (2.16)–(2.18) into eqn. (2.15) to derive expressions for the normal and tangential projections of eqn. (2.15) with respect to the bilayer surface (*cf.* refs. 61 and 68)

$$b_{\mu\nu}\sigma^{\mu\nu} + \sigma^{\nu(n)}_{,\nu} = [(P_N - P_T)|\nabla_{II}\zeta|^2 - \Pi](1 + |\nabla_{II}\zeta|^2)^{-1} + \Pi_0 + \boldsymbol{n} \cdot \boldsymbol{\tau} \cdot \boldsymbol{n} \tag{2.19}$$

$$\sigma^{\mu\nu}_{,\mu} - b^{\nu}_{\mu}\sigma^{\mu(n)} = (P_T - P_N - \Pi)(1 + |\nabla_{II}\zeta|^2)^{-1/2}\zeta^{,\nu} + \boldsymbol{n} \cdot \boldsymbol{\tau} \cdot \boldsymbol{a}^{\nu}; \qquad \nu = 1, 2 \tag{2.20}$$

where the comma denotes covariant differentiation;[69] $b_{\mu\nu}$ are components of the curvature tensor, and $\Pi_0 = P_0 - P_N$ is the disjoining pressure of the non-deformed plane-parallel bilayer. The requirement for balance of the interfacial angular momentum implies[61,67,68]

$$\sigma^{\mu(n)} = -M^{\mu\nu}_{,\nu} \tag{2.21}$$

where $M^{\mu\nu}(\mu, \nu = 1, 2)$ represent components of the tensor of the interfacial moments (torques). Assuming that the bilayer surfaces behave like a two-dimensional fluid we require lateral isotropy of the interfacial stresses

$$\sigma_{\mu\nu} = \sigma a_{\mu\nu} \qquad (a_{\mu\nu} \equiv \boldsymbol{a}_\mu \cdot \boldsymbol{a}_\nu) \tag{2.22}$$

where σ is the bilayer surface tension.

Hereafter we will assume small deformations. Then Π can be expanded in series:

$$\Pi = \Pi_0 + 2\Pi'\zeta + \ldots; \qquad \Pi' \equiv \left(\frac{\mathrm{d}\Pi}{\mathrm{d}h}\right)_{\zeta=0} \tag{2.23}$$

Moreover, for small deformations the bilayer surfaces can be treated as Helfrich interfaces for which

$$M^{\mu\nu}_{,\nu} = 2k_c H^{,\mu} - (B_0'/h)\zeta^{,\mu} \tag{2.24}$$

[see Appendix B for the derivation of eqn. (2.24)]; the meaning of B_0' is the same as in eqn. (1.20). Here H is the interfacial mean curvature. Note that[61,70]

$$2H = a^{\mu\nu}b_{\mu\nu} \approx \nabla_{II}^2\zeta \tag{2.25}$$

where the last relation holds in linear approximation for small ζ. Next by using eqn. (2.4*b*), (2.8) and (2.21)–(2.25) we obtain the linearised form of eqn. (2.19),

$$\tilde{\sigma}_0 \nabla_{II}^2\zeta - k_c\nabla_{II}^4\zeta = 2(\lambda/h - \Pi')\zeta; \qquad (\tilde{\sigma}_0 \equiv \sigma_0 + B_0'/h) \tag{2.26}$$

where σ_0 is the value of σ for the non-disturbed plane-parallel bilayer. Eqn. (2.26) can be represented in the form

$$(\nabla_{II}^2 - q_2^2)(\nabla_{II}^2 - q_1^2)\zeta = 0 \tag{2.27}$$

where q_1^2 and q_2^2 are roots of the biquadratic equation

$$k_c q^4 - \tilde{\sigma}_0 q^2 + 2(2\lambda/h - \Pi') = 0 \tag{2.28}$$

i.e.,

$$q_{1,2}^2 = \frac{1}{2k_c}\{\tilde{\sigma}_0 \pm [\tilde{\sigma}_0^2 - 8k_c(2\lambda/h - \Pi')]^{1/2}\} \tag{2.29}$$

Depending on the sign of the discriminant in eqn. (2.29), eqn. (2.28) may have four real or four complex roots. We can eliminate in advance all roots which give negative q^2, which correspond to an infinitely large energy of insertion and inclusion in the bilayer. [One can prove that in the latter case $\zeta \propto J_0(qr)$ around a single inclusion; then the total energy of deformation turns out to be infinite because of the slow rate of decay of the Bessel function J_0 at infinity.] The complex

roots for q lead to decaying oscillatory profiles, resembling those obtained in ref. 47 for model inclusions of translational symmetry.

As $\tilde{\sigma}_0$ (and possibly k_c and λ) depends strongly on temperature and total membrane tension γ_b, various types of solutions are possible. Below we restrict our considerations to the case of not-too-flaccid membranes, when σ_0 is large enough to provide a positive discriminant in eqn. (2.29), *i.e.*

$$\tilde{\sigma}_0^2 > 8k_c(2\lambda/h - \Pi') \tag{2.30}$$

All other cases can be treated similarly by using the methodology developed below.

The estimates show that Π' is typically about 2×10^{13} N m^{-3} and is negligible compared with $2\lambda/h$. With $\lambda = 2 \times 10^6$ Pa, $h = 3$ nm and $k_c \approx kT \approx 4 \times 10^{-21}$ J (see ref. 71), eqn. (2.30) yields $\tilde{\sigma}_0 > 6.5$ mN m^{-1}.

q^{-1} is the capillary length, determining the range of the deformation around an inclusion and in turn, the range of the lateral capillary forces between inclusions (see below). With the above values and $\tilde{\sigma}_0 = 20$ mN m^{-1} from eqn. (2.29) two possible decay lengths can be calculated: $q_1^{-1} = 2.7$ nm and $q_2^{-1} = 0.45$ nm. There is a physical and a mathematical reason to disregard the second root, q_2: (i) From a physical viewpoint a decay length smaller than the size of a lipid headgroup (typically 0.8 nm) does not make sense. (ii) From a mathematical viewpoint the present linearised theory is valid when $(qh_c)^2 \ll 1$, see eqn. (3.6) below; this requirement may be violated with $q = q_2$. Consequently, we will work with

$$q^2 = q_1^2 = \frac{1}{2k_c}\{\tilde{\sigma}_0^2 - [\tilde{\sigma}_0^2 - 8k_c(2\lambda/h) - \Pi']^{1/2}\}$$

$$\approx 4\lambda/(h\tilde{\sigma}_0) \tag{2.31}$$

The last approximate expression is obtained by expanding the square root in eqn. (2.29) in series for small k_c. In addition, disregarding the solutions of eqn. (2.27) with $q = q_2$ implies that ζ must satisfy the equation

$$\nabla_{II}^2 \zeta = q^2 \zeta \tag{2.32}$$

where q is given by eqn. (2.31). Indeed, all solutions of eqn. (2.32) satisfy eqn. (2.27), and all solutions of eqn. (2.27) of decay length q_1 obey eqn. (2.32). Eqn. (2.32) is to be solved in conjunction with two physical boundary conditions: $\zeta = h_c$ at the lipid–protein boundary and $\zeta \to 0$ for $r \to 0$, see Fig. 5.

Comparison between eqn. (2.12) and (2.32) shows that one can obtain g in the form

$$g = \frac{1}{bq^2}\zeta + f(x, y, z) \tag{2.33}$$

where the unknown function f satisfies the homogeneous equation

$$\nabla_{II}^2 f = 0 \tag{2.34}$$

Deformation around a Single Inclusion

In the case of a single cylindrical inclusion (Fig. 5) ζ depends only on the radial coordinate r, and eqn. (2.32) reduces to

$$\frac{1}{r}\frac{d}{dr}\left(r\frac{d\zeta}{dr}\right) = q^2\zeta \tag{3.1}$$

The solution of eqn. (3.1) along with the boundary condition for constant elevation at the contact line (see Fig. 5),

$$\zeta = h_c = \text{const. (at the contact line)} \tag{3.2}$$

yields

$$\zeta = \frac{h_c}{K_0(qr_c)}K_0(qr); \qquad r \geqslant r_c \tag{3.3}$$

where r_c is the radius of the cylindrical inclusion and K_0 is a modified Bessel function, see *e.g.* ref. 72 and 73. The boundary condition of eqn. (2.14) in conjunction with eqn. (2.33) leads to

$$\left(\frac{1}{bq^2}\frac{\partial\zeta}{\partial r} + \frac{\partial f}{\partial r}\right)_{r=r_c} = 0 \tag{3.4}$$

From eqn. (2.34) one obtains

$$f = A \ln r \tag{3.5}$$

where A is a constant of integration; it is to be determined from the boundary condition

$$\left.\frac{\partial\zeta}{\partial r}\right|_{r=r_c} = -\tan\Psi_c = -qh_c\frac{K_1(qr_c)}{K_0(qr_c)} \tag{3.6}$$

Here Ψ_c is the surface slope at the contact line (Fig. 5). From eqn. (3.4)–(3.6) one determines

$$A = (2r_c \tan\Psi_c)/(hq^2) \tag{3.7}$$

Further, by using eqn. (2.11), (2.33), (3.5) and (3.7) one can calculate the components of the displacement vector $\boldsymbol{u}$:

$$u_r = \frac{-2}{hq^2}\left(\frac{\partial\zeta}{\partial r} + \frac{r_c}{r}\tan\Psi_c\right); \qquad u_\phi = 0 \tag{3.8}$$

u_z and ζ are determined by eqn. (2.8) and (3.3), respectively. Finally, one can calculate the components of the strain tensor in cylindrical coordinates by using standard formulae:[59]

$$u_{rr} = \frac{\partial u_r}{\partial r} = \frac{-2}{hq^2}\left(\frac{\partial^2\zeta}{\partial r^2} - \frac{r_c}{r^2}\tan\Psi_c\right) \tag{3.9}$$

$$u_{\phi\phi} = \frac{u_r}{r} = \frac{-2}{hq^2}\left(\frac{1}{r}\frac{\partial\zeta}{\partial r} + \frac{r_c}{r^2}\tan\Psi_c\right) \tag{3.10}$$

$$u_{zz} = \frac{\partial u_z}{\partial z} = \frac{2\zeta}{h}; \qquad u_{rz} = \frac{z}{h}\frac{\partial\zeta}{\partial r}; \qquad u_{r\phi} = u_{\phi z} = 0 \tag{3.11}$$

Deformation around Two Inclusions

We consider two membrane proteins (Fig. 6) whose lateral surfaces are modelled as two identical circular cylinders of radius r_c. Their axes of symmetry are separated at a distance L. The contact lines are attached to the boundaries between the hydrophilic and hydrophobic regions on the protein surface; therefore the elevation h_c (unlike the running slope angle Ψ_c) does not change with the variation of L.

The geometry of the system suggests introduction of orthogonal bipolar coordinates[73] in the plane xy:

$$x = \frac{a\sinh\tau}{\cosh\tau - \cos\omega}; \qquad y = \frac{a\sin\omega}{\cosh\tau - \cos\omega}$$

$$-\infty < \tau < +\infty \qquad -\pi \leqslant \omega \leqslant \pi \tag{4.1}$$

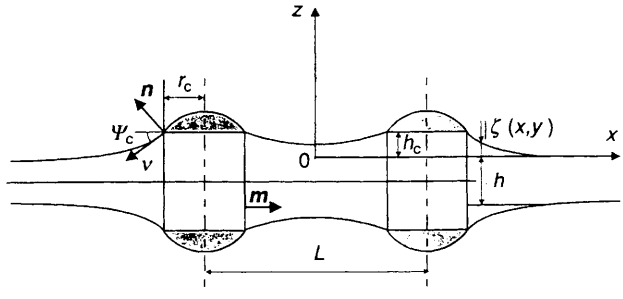

Fig. 6 Two identical cylindrical inclusions of radius r_c separated at an axis-to-axis distance L; h_c characterises the 'mismatch' between the width of the inclusion hydrophobic belt and the thickness of the bilayer far from the inclusion

Each line $\tau = \text{const.}$ is a circumference,[73]

$$(x - a \coth \tau)^2 + y^2 = \frac{a^2}{\sinh^2 \tau} \tag{4.2}$$

see Fig. 7. Let $\tau = \pm\tau_c$ be the equation of the intersection lines of the two cylinders with the plane xy. Then in accordance with eqn. (4.2) one finds

$$r_c = a/\sinh \tau_c; \qquad L = 2a \coth \tau_c \tag{4.3}$$

The elimination of τ_c yields an expression for the parameter a in eqn. (4.1):

$$a = (L^2/4 - r_c^2)^{1/2} \tag{4.4}$$

(see also Fig. 7).

In bipolar coordinates eqn. (2.32) takes the form[73]

$$(\cosh \tau - \cos \omega)^2 \left(\frac{\partial^2 \zeta}{\partial \tau^2} + \frac{\partial^2 \zeta}{\partial \omega^2} \right) = (aq)^2 \zeta(\tau, \omega) \tag{4.5}$$

Eqn. (4.5) is to be solved along with the boundary condition eqn. (3.2). When $(aq)^2 \ll 1$ one can use perturbation methods to solve eqn. (4.5).[48,49] Here we prefer to use numerical integration of eqn. (4.5), which can be carried out for any value of $(aq)^2$ as described below.

The domain of integration of eqn. (4.5) represents a rectangle in the $\tau\omega$-plane, which is bounded by the lines $\omega = \pm\pi$ and $\tau = \pm\tau_c$; in view of eqn. (4.3) we have

$$\tau_c = \ln\left[\frac{a}{r_c} + \sqrt{\left(\frac{a^2}{r_c^2} + 1 \right)} \right] \tag{4.6}$$

Owing to the symmetry we consider only a quarter of the integration domain, that with $0 \leqslant \tau \leqslant \tau_c$ and $0 \leqslant \omega \leqslant \pi$. The additional boundary conditions implied by the symmetry are

$$\left.\frac{\partial \zeta}{\partial \tau}\right|_{\tau=0} = \left.\frac{\partial \zeta}{\partial \omega}\right|_{\omega=0} = \left.\frac{\partial \zeta}{\partial \omega}\right|_{\omega=\pi} = 0 \tag{4.7}$$

We used the classical second-order finite-difference scheme for discretisation of the boundary problem.[73,74] Thus eqn. (4.5) is represented as a system of linear equations which can be solved by means of one of the standard methods. We used the Gauss–Seidel iterative method[73,74] combined with successive over-relaxation (SOR) and Chebyshev acceleration techniques, see *e.g.* ref. 74 and 75.

Consideration of symmetry shows that $f(\tau, \omega)$ is an even function of both τ and ω. Therefore, the solution of eqn. (2.34) can be presented in the form

$$f(\tau, \omega) = \sum_{n=1}^{\infty} E_n \cosh n\tau \cos n\omega \tag{4.8}$$

The coefficients E_n can be determined by substituting eqn. (4.8) and (2.33) into the boundary condition, eqn. (2.14)

$$E_n = \frac{1}{n\pi bq^2 \sinh n\tau_c} \int_{-\pi}^{\pi} d\omega \cos n\omega \left.\frac{\partial \zeta}{\partial \tau}\right|_{\tau=\tau_c} \tag{4.9}$$

Next, one can determine the components of the displacement vector $\boldsymbol{u}$ from eqn. (2.8), (2.11), (2.33), (4.8) and (4.9).

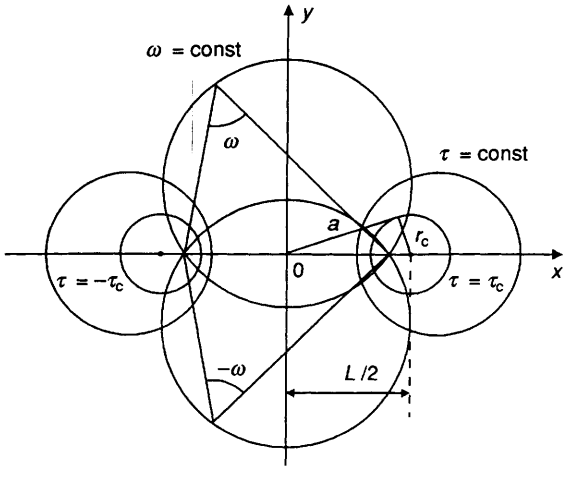

Fig. 7 Bipolar coordinates (τ, ω) in the plane xy. The circumferences $\tau = \pm\tau_c$ represent projections of the lateral surfaces of the two cylindrical inclusions (Fig. 6).

Lateral Capillary Force between Two Identical Inclusions

Force Approach

The lateral capillary force exerted on an inclusion in a lipid bilayer, like those depicted in Fig. 6, can be calculated by integrating the surface and bulk stress tensors, along the contact lines and particle surfaces:[49]

$$\boldsymbol{F} = 2\boldsymbol{U}_{II} \cdot \oint_C d\boldsymbol{l}\boldsymbol{\nu} \cdot \boldsymbol{\sigma} + \boldsymbol{U}_{II} \cdot \int_S d\boldsymbol{s}\boldsymbol{m} \cdot \boldsymbol{\tau} \tag{5.1}$$

Here C denotes the contact line; the multiplier 2 accounts for the presence of two identical contact lines on each inclusion; dl and ds are scalar linear and surface elements; $\boldsymbol{\nu}$ is a unit vector which is simultaneously normal to the contour C and tangential to the bilayer surface (Fig. 6); S is the lateral surface of the cylindrical inclusion and $\boldsymbol{m}$ is its outer-running unit normal. It should be noted that in the case of a single inclusion in the bilayer both integrals in eqn. (5.1) are equal to zero owing to the symmetry of the exerted stresses. However, the presence of a second inclusion (Fig. 6) breaks the symmetry and leads to a non-zero lateral capillary force $\boldsymbol{F}$. By means of eqn. (2.21), (2.24), (2.25) and (2.32) one can derive

$$\sigma^{\mu(n)} = -M^{\mu\nu}_{,\nu} = -(k_c q^2 - B_0'/h)\zeta_{,\mu} \tag{5.2}$$

Then by using eqn. (2.18), (2.22), (5.1) and (5.2) one can formally present the lateral force $\boldsymbol{F}$ as a sum of contributions due to the surface tension, $\boldsymbol{F}^{(\sigma)}$, interfacial bending moment, $\boldsymbol{F}^{(B)}$, and stresses in the bilayer interior, $\boldsymbol{F}^{(i)}$:

$$\boldsymbol{F}^{(\sigma)} = 2 \oint_C d\boldsymbol{l}(\boldsymbol{U}_{II} \cdot \boldsymbol{\nu})\sigma \tag{5.3}$$

$$\boldsymbol{F}^{(B)} = -2(k_c q^2 - B_0'/h) \oint_C d\boldsymbol{l}\boldsymbol{\nu} \cdot \nabla_s \zeta(\boldsymbol{U}_{II} \cdot \boldsymbol{n}) \tag{5.4}$$

$$\boldsymbol{F}^{(i)} = \int_S d\boldsymbol{s}\boldsymbol{m} \cdot \boldsymbol{\tau} \cdot \boldsymbol{U}_{II}$$

First we note that in bipolar coordinates the last equation reads

$$\boldsymbol{F}^{(i)} = -\int_S ds(\tau_{\tau\tau}\boldsymbol{e}_\tau + \tau_{\tau\omega}\boldsymbol{e}_\omega) = 0 \tag{5.5}$$

because $\tau_{\tau\tau} = -p = 0$ and $\tau_{\tau\omega} = 0$, *cf.* eqn. (2.4*a*) and (2.13). The fact that $\boldsymbol{F}^{(i)} = 0$ could be anticipated in so far as the lateral stresses in the bilayer have been assumed to be isotropic (condition for two-dimensional fluidity) and the contact lines are parallel to the bilayer midsurface, see Fig. 6.

Simple geometrical considerations (Fig. 6) yield

$$\boldsymbol{U}_{II} \cdot \boldsymbol{\nu} = \boldsymbol{m} \cos \Psi_c; \qquad \boldsymbol{U}_{II} \cdot \boldsymbol{n} = \boldsymbol{m} \sin \Psi_c \tag{5.6}$$

In addition, by using eqn. (2.16), one obtains

$$\sin \Psi_c = \boldsymbol{m} \cdot \boldsymbol{n} = \frac{-\boldsymbol{m} \cdot \nabla_{II} \zeta}{(1 + |\nabla_{II} \zeta|^2)^{1/2}}\bigg|_{\tau=\tau_c};$$
$$\cos \Psi_c = \boldsymbol{e}_z \cdot \boldsymbol{n} = (1 + |\nabla_{II} \zeta|^2)_{\tau=\tau_c}^{-1/2} \quad (5.7)$$

It can be proven that

$$\boldsymbol{v} \cdot \nabla_s \zeta = \frac{\boldsymbol{m} \cdot \nabla_{II} \zeta}{\sqrt{(1 + |\nabla_{II} \zeta|^2)}} \quad (5.8)$$

(at the inclusion contact line).

The substitution of eqn. (5.6)–(5.8) into eqn. (5.3) and (5.4) leads to

$$\boldsymbol{F}^{(\sigma)} = 2 \oint_C d\boldsymbol{l}\boldsymbol{m}(1 + |\nabla_{II} \zeta|^2)^{-1/2}\sigma \quad (5.9)$$

$$\boldsymbol{F}^{(B)} = 2(k_c q^2 - B_0'/h) \oint_C d\boldsymbol{l}\boldsymbol{m}(\boldsymbol{m} \cdot \nabla_{II} \zeta)^2 \times (1 + |\nabla_{II} \zeta|^2)^{-1} \quad (5.10)$$

As we work with small deformations, we will keep only linear and quadratic terms (with respect to deformation) in the right-hand sides of eqn. (5.9) and (5.10) and we will neglect higher-order terms.

Thus for the x-projection of $\boldsymbol{F}^{(B)}$ we obtain

$$F_x^{(B)} \equiv \boldsymbol{e}_x \cdot \boldsymbol{F}^{(B)} = 2(k_c q^2 - B_0'/h) \times \oint_C dl\, |\nabla_{II} \zeta|^2 \cos \phi \quad (5.11)$$

where we have used the relationships

$$\cos \phi \equiv \boldsymbol{e}_x \cdot \boldsymbol{m}; \qquad \boldsymbol{m} \cdot \nabla_{II} \zeta = -|\nabla_{II} \zeta|_{\tau=\tau_c} \quad (5.12)$$

In fact, $|F_x^{(B)}| = |\boldsymbol{F}^{(B)}|$ because of the symmetry of the system.

Next we proceed with $\boldsymbol{F}^{(\sigma)}$. In Appendix B we prove that the dependence of σ on the deformation can be represented in the form

$$\sigma = \sigma_0 - \tfrac{1}{2}(k_c q^2 - B_0'/h)|\nabla_{II} \zeta|^2 + (P_T - P_0)\zeta + (\lambda/h - \Pi')\zeta^2 \quad (5.13)$$

Taking into account that $\zeta = h_c = \text{const.}$ at the contour C, from eqn. (5.9) and (5.13) we derive

$$F_x^{(\sigma)} = -(\sigma_0 + k_c q^2 - B_0'/h) \oint_C dl\, |\nabla_{II} \zeta|^2 \cos \phi \quad (5.14)$$

where higher-order terms are neglected. It is convenient to use ω as the integration variable. One can write[49]

$$dl = \chi\, d\omega; \qquad \cos \phi = \frac{\chi}{a}(\cosh \tau_c \cos \omega - 1);$$
$$\nabla_{II} \zeta = \boldsymbol{e}_\tau \frac{1}{\chi} \frac{\partial \zeta}{\partial \tau}; \qquad \text{for } \tau = \tau_c \quad (5.15)$$

where

$$\chi = \frac{a}{\cosh \tau - \cos \omega} \quad (5.16)$$

By using eqn. (5.5), (5.11) and (5.14)–(5.16) one derives the desired expression for the lateral capillary force

$$F_x \equiv F_x^{(B)} + F_x^{(\sigma)} + F_x^{(i)} = -\frac{2}{a}(\tilde{\sigma}_0 - k_c q^2) \int_0^\pi d\omega(\cosh \tau_c \cos \omega - 1)\left(\frac{\partial \zeta}{\partial \tau}\right)_{\tau=\tau_c}^2 \quad (5.17)$$

Note that the force F_x can be attractive or repulsive depending on whether $\tilde{\sigma}_0 > k_c q^2$ or $\tilde{\sigma}_0 < k_c q^2$. To calculate F_x we first solve eqn. (4.5) numerically to determine the derivative $\partial \zeta / \partial \tau$ for $\tau = \tau_c$ and then we carry out the integration in eqn. (5.17), again numerically. A subsequent integration yields the interaction energy between the two inclusions separated at a distance L:

$$\Delta\Omega(L) = \int_L^\infty F_x(L)\, dL \quad (5.18)$$

An alternative approach, presented below, allows one to calculate directly the interaction energy $\Delta\Omega$.

Energy Approach

First note that the macroscopic theory (mechanics and thermodynamics) provides a general expression for the variation of the grand thermodynamic potential, $\delta\Omega$, rather than for Ω itself. In principle, one can find Ω by integrating $\delta\Omega$, but such an integration is straightforward only for fluid phases or isotropic elastic bodies.

In the case of curved interfaces $\delta\Omega$ depends on three independent variations: ζ, u_x and u_y, see *e.g.* ref. 77, eqn. (5.7)–(5.8). In our case, the solution of the mechanical problem for the bilayer interior, coupled with the respective boundary conditions at the bilayer surfaces, leads to connections between u_x, u_y and ζ. These connections allow one to obtain *a posteriori* an expression for Ω in terms of ζ only. As demonstrated in Appendix C for the system under consideration (Fig. 6) this expression reads

$$\Omega = \int_{S_0} ds[(\tilde{\sigma}_0 - k_c q^2)|\nabla_{II} \zeta|^2 + 2(2\lambda/h - \Pi')\zeta^2] + \text{const.} \quad (5.19)$$

where higher order terms are neglected; S_0 denotes the whole area of the plane xy except the area excluded by the inclusions; the additive constant in eqn. (5.19) does not depend on the bilayer deformation. By using the identity

$$|\nabla_{II} \zeta|^2 = \nabla_{II} \cdot (\zeta \nabla_{II} \zeta) - \zeta \nabla_{II}^2 \zeta$$

and the Green integral theorem,[69] we may write eqn. (5.19) in a new form

$$\Omega = 2(\tilde{\sigma}_0 - k_c q^2) \oint_C dl(-\boldsymbol{m}) \cdot (\zeta \nabla_{II} \zeta) - \int_{S_0} ds[\tilde{\sigma}_0 \nabla_{II}^2 \zeta - k_c q^2 \nabla_{II}^2 \zeta - 2(2\lambda/h - \Pi')\zeta]\zeta$$

The integrand of the surface integral is identically zero; *cf.* eqn. (2.26) and (2.32). Next we utilise eqn. (3.2) to obtain

$$\Omega(L) = 4\pi(\tilde{\sigma}_0 - k_c q^2) r_c h_c \tan \Psi_c(L) \quad (5.20)$$

where

$$\tan \Psi_c(L) \equiv \frac{1}{2\pi r_c} \oint_C dl(-\boldsymbol{m} \cdot \nabla_{II} \zeta) = \frac{1}{2\pi r_c} \int_{-\pi}^{\pi} d\omega \frac{\partial \zeta}{\partial \tau}\bigg|_{\tau=\tau_c} \quad (5.21)$$

represents the average meniscus slope at the contact line. Finally, the inclusion–inclusion interaction energy is

$$\Delta\Omega(L) \equiv \Omega(L) - \Omega(\infty) = 4\pi(\tilde{\sigma}_0 - k_c q^2) \times r_c h_c[\tan \Psi_c(L) - \tan \Psi_c(\infty)] \quad (5.22)$$

where angle $\Psi_c(\infty)$ is determined by eqn. (3.6). To determine $\Psi_c(L)$ we carry out the integration in eqn. (5.21) numerically. As proven analytically in Appendix C, eqn. (5.18) and (5.22) are equivalent, *i.e.* they must give the same curves $\Delta\Omega$ *vs.* L. This fact can be used to check the precision of the numerical procedure.

To calculate $\Delta\Omega(L)$ from eqn. (5.22) one is first to solve numerically eqn. (4.5) and then to substitute the calculated $\partial\zeta/\partial\tau$ in the right-hand side of eqn. (5.21). In Appendix D we derive an asymptotic formula for $\Delta\Omega(L)$, which reads

$$\Delta\Omega(L) = 4\pi(\tilde{\sigma}_0 - q^2k_c)qr_c h_c^2 \times \left[\frac{K_1(qr_c) - \frac{1}{2}qr_c K_0(qL)}{K_0(qr_c) + K_0(qL)} - \frac{K_1(qr_c)}{K_0(qr_c)}\right] \quad (5.23)$$

The numerical test of eqn. (5.23) shows that it gives $\Delta\Omega(L)$ with a good accuracy (see Fig. 12). For $L \gg r_c$ one can expand the denominator of eqn. (5.23) in series and keep the linear term to get a simpler expression:

$$\Delta\Omega(L) = -4\pi(\tilde{\sigma}_0 - q^2k_c)\frac{qr_c h_c^2}{K_0(qr_c)} \times \left[\frac{K_1(qr_c)}{K_0(qr_c)} + \frac{qr_c}{2}\right]K_0(qL) \quad (5.24)$$

Eqn. (5.24) represents a good approximation for any L except for $L < 3r_c$, when it gives a more negative $\Delta\Omega$ than the exact result. The lateral capillary force can be obtained by differentiation:

$$F_x = -\frac{\partial\Delta\Omega}{\partial L}$$

Numerical Results and Discussion

In this section we present results from numerical calculations of the capillary interaction energy and force between two membrane proteins incorporated into a flat lipid bilayer. In our model calculations we used the parameters of the bacteriorhodopsin molecule, which has approximately cylindrical shape (see *e.g.* ref. 1 and 76). The geometrical parameters of this cylindrical molecule are known from electron microscopy studies[1,76] to be $r_c = 1.5$ nm and $l_0 = 3.0$ nm (*cf.* Fig. 5). We suppose that the hydrophobic α-helix regions of the bacteriorhodopsin molecule are situated entirely inside the lipid bilayer. The respective 'three-phase contact lines' are situated between the hydrophobic wall of the cylinder (formed from packed α-helix chains) and its hydrophilic parts (the bases of the cylinder). As earlier we use typical values for the bilayer parameters: $\lambda = 2 \times 10^6$ N m^{-2}, $\sigma_0 = 35$ mN m^{-1} and $B_0' = -3.2 \times 10^{-11}$ N [see eqn. (A.29) and (A.20) in Appendix A].

As an illustration in Fig. 8 we have plotted the calculated bilayer shape around two bacteriorhodopsin molecules at fixed distance $L = 4r_c$. Fig. 8(a) and (b) correspond to positive and negative h_c, respectively. Note that $h_c = (l_0 - h)/2$. One can see from these figures that the bilayer shape perturbation is short-ranged and comparable with the capillary length $q^{-1} = 2.15$ nm.

Our results for the lateral capillary force *vs.* $L/2r_c$ for different bilayer thicknesses, h, are shown in two plots: Fig. 9(a) for $h_c > 0$ and Fig. 9(b) for $h_c < 0$. The values of h correspond to the thicknesses of the bilayer[9] (studied experimentally in ref. 27). One sees that in both cases the capillary force is negative and corresponds to attraction between the protein molecules in the bilayer. Comparing the cases when h_c has the same magnitude but the opposite signs [note that $h_c = 0.2$ nm for the curve with $h = 2.6$ nm in Fig. 9(a), whereas $h_c = -0.2$ nm

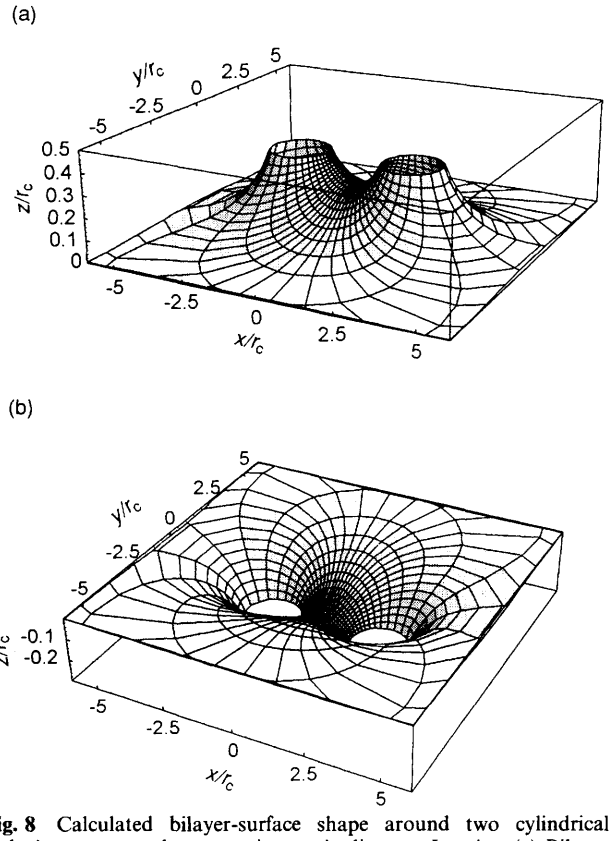

Fig. 8 Calculated bilayer-surface shape around two cylindrical inclusions separated at an axis-to-axis distance $L = 4r_c$. (a) Bilayer surface is convex, $h_c/r_c = 0.35$; (*b*) bilayer surface is concave, $h_c/r_c = -0.28$. $\lambda = 2 \times 10^6$ N m^{-2}, $B_0' = -3.2 \times 10^{-11}$ N, $h = 1.95$ nm and $\sigma_0 = 35$ mN m^{-1}.

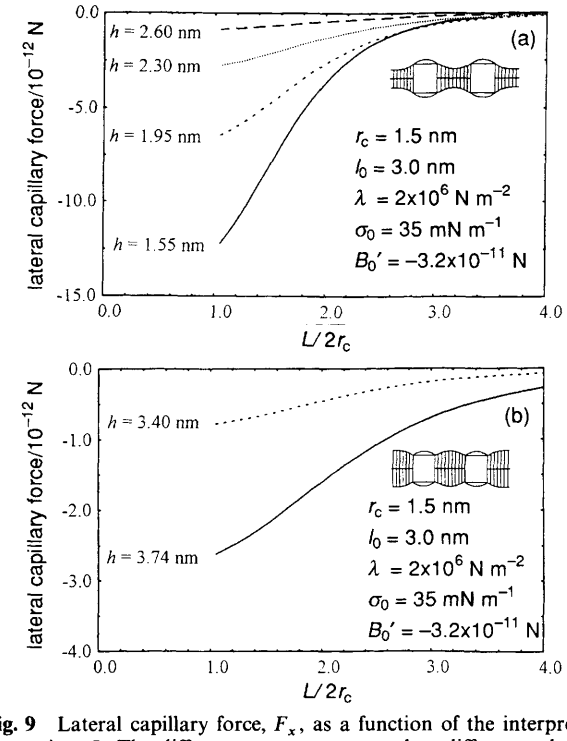

Fig. 9 Lateral capillary force, F_x, as a function of the interprotein separation, L. The different curves correspond to different values of the bilayer thickness, h. The geometrical parameters of the protein molecules are taken from ref. 27: $r_c = 1.5$ nm and $l_0 = 3.0$ nm; $\lambda = 2 \times 10^6$ N m^{-2}, $B_0' = -3.2 \times 10^{-11}$ N, $\sigma_0 = 35$ mN m^{-1}. The bilayer is thinner (a) or thicker (b) than the bacteriorodopsin hydrophobic zone.

for the curve with $h = 3.4$ nm in Fig. 9(b)], one can conclude that the capillary attraction is larger by magnitude and more long-ranged in the case of $h_c < 0$ (thicker bilayer). This finding is consonant with the observations of Lewis and Engelman.[27]

Fig. 10(a) and (b) represent the respective capillary interaction energy $\Delta\Omega$ *vs.* the dimensionless distance, $L/2r_c$ at the same value of h as in Fig. 9(a) and (b). Here and hereafter we compare $\Delta\Omega$ with the energy of the thermal motion, kT, for $T = 298$ K. One can see that both for $h_c > 0$ and $h_c < 0$ the interaction energy is larger than the thermal energy, kT, except for $h = 2.60$ nm and $h = 3.40$ nm, corresponding to rather small values of h_c. However, for the two limiting cases, $h = 1.55$ nm and $h = 3.75$ nm, the interaction energy is high enough (5–10 kT in close contact) to cause an aggregation of the membrane proteins. Only in these two limiting cases did Lewis and Engelman[27] observe protein aggregation.

Fig. 11 illustrates the dependence of $\Delta\Omega$ on h_c for a fixed separation, $L = 2r_c$, between the axes of the two proteins (close contact). The minimum for $h_c = 0$ should be expected. The three curves correspond to three different values of the surface tension, σ_0. Note that the magnitude of the capillary interaction energy increases with the increase of σ_0. Besides, the interaction is stronger for the case when the bilayer is thicker than the protein hydrophobic zone ($h_c < 0$), as noted above.

In conclusion, we note that Fig. 9–11 give an illustration of the order of magnitude and range of the protein–protein interactions, rather than a quantitative comparison between theory and experiment. The real experiment is too complicated and many parameter values are unknown; *e.g.* the temperature (and consequently the values of σ_0, λ, *etc.*) are different in the separate experiments[27] with bilayers of different thicknesses.

Finally, we note that the two alternative procedures for calculating $\Delta\Omega(L)$ based on eqn. (5.17), (5.18), (5.21) and (5.22) give coinciding numerical results as expected. These procedures have been used to calculate the curves in Fig. 10 and 11. In addition, in Fig. 12 the asymptotic formula, eqn. (5.23), is compared with the exact output of eqn. (5.21) and (5.22). One sees that the asymptotic formula provides good accuracy.

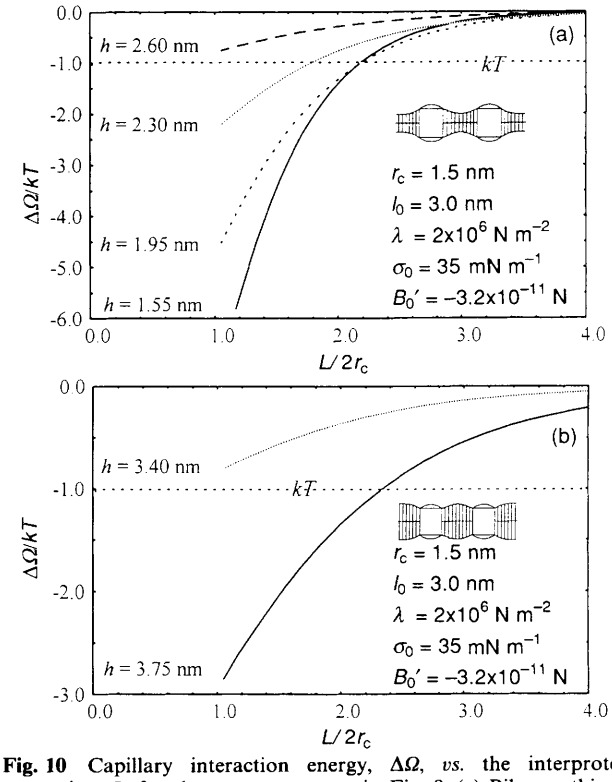

Fig. 10 Capillary interaction energy, $\Delta\Omega$, *vs.* the interprotein separation, L, for the same system as in Fig. 9. (a) Bilayers thinner and (b) thicker than the hydrophobic belt of the protein.

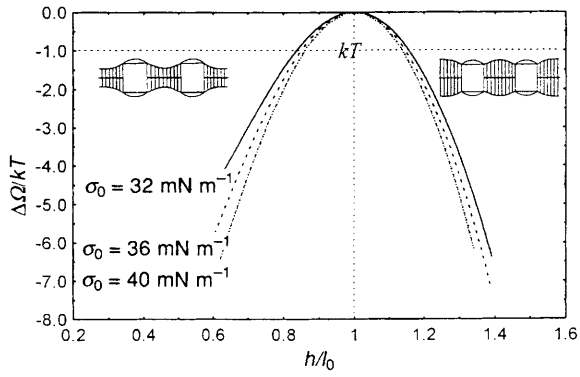

Fig. 11 Capillary interaction energy, $\Delta\Omega$, of two proteins in close contact ($L/r_c = 2$) as a function of the bilayer thickness, h. The three curves correspond to different values of the surface tension, σ_0. The values of the other parameters are the same as in Fig. 9.

Comparison with the Theory described in Ref. 47

Our aim is to compare our model with that by Dan *et al.*[47] and to check whether the phenomenological parameters used in these two studies can be related. The model by Dan *et al.*[47] is based on an expression for the free energy (per lipid molecule) of a curved lipid monolayer:

$$f(\zeta, \Sigma) = f_0(\Sigma) + \kappa(\Sigma)\frac{d^2\zeta}{dx^2} + K_d(\Sigma)\left(\frac{d^2\zeta}{dx^2}\right)^2 \qquad (6.1)$$

where Σ is the surface area per molecule. These authors consider the simpler case of translational symmetry, that is the bilayer profile in Fig. 6 is translated along the y-axis; consequently $\zeta = \zeta(x)$. The comparison between eqn. (6.1) and the Helfrich[78] expression for the energy of flexural deformation yields

$$k_c = 2K_d/\Sigma \qquad (6.2)$$

Further, Dan *et al.*[47] obtain an expression for the change in the monolayer energy (per unit length along the y-axis) due

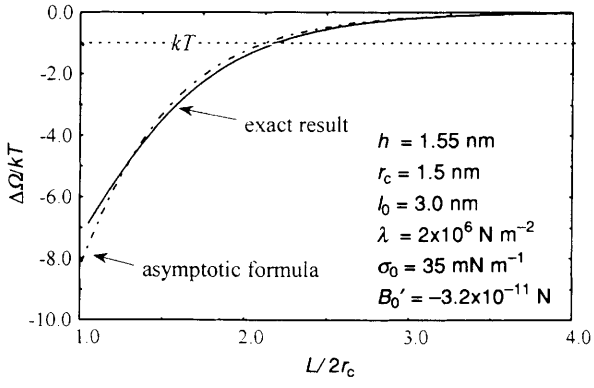

Fig. 12 Comparison of the $\Delta\Omega$ *vs.* L curves calculated by means of eqn. (5.22) and the asymptotic formula, eqn. (5.23)

to insertion of two inclusions:

$$F_d = \int_0^L dx\left[\frac{f_0''\Sigma}{2b^2}\zeta^2 + \frac{\kappa}{\Sigma}\frac{d^2\zeta}{dx^2} + \left(\frac{\kappa}{\Sigma} - \kappa'\right)\frac{\zeta}{b}\frac{d^2\zeta}{dx^2} + \frac{K_d}{\Sigma}\left(\frac{d^2\zeta}{dx^2}\right)^2\right] \quad (6.3)$$

where $b \equiv h/2$ and the prime denotes $\partial/\partial\Sigma$. By variations from eqn. (6.3) one derives an equation for ζ:

$$\frac{2}{b}\left(\kappa' - \frac{\kappa}{\Sigma}\right)\frac{d^2\zeta}{dx^2} - \frac{2K_d}{\Sigma}\frac{d^4\zeta}{dx^4} = \frac{f_0''\Sigma}{b^2}\zeta \quad (6.4)$$

Comparing eqn. (6.4) with eqn. (2.26) for $\nabla_\Pi = e_x\partial/\partial x$ and keeping in mind eqn. (6.2) one obtains

$$\lambda = \frac{f_0''\Sigma}{2b} + b\Pi' \quad (6.5)$$

$$\tilde{\sigma}_0 \equiv \sigma_0 + B_0'/h = \frac{2}{b}\left(\kappa' - \frac{\kappa}{\Sigma}\right); \quad h = 2b \quad (6.6)$$

In ref. 47 expressions for $f_0(\Sigma)$, $\kappa(\Sigma)$ and $K_d(\Sigma)$ in terms of molecular parameters are provided; the substitution of these expression into eqn. (6.2), (6.5) and (6.6) yields

$$\lambda = \frac{3a_1kT}{\Sigma^2}; \qquad \tilde{\sigma}_0 = \frac{16a_2b\tilde{\varepsilon}kT}{\Sigma^2};$$

$$k_c = \frac{a_3b^3kT}{2\Sigma^2}(1 + 12\tilde{\varepsilon}^2) \quad (6.7)$$

where the Π'-term is neglected; $a_1 = a\pi^2/24$, $a_2 = a_3 = a\pi^2/32$, a is a molecular length scale; the molecular parameters are appropriate for amphiphiles as $(C_2H_4)_n(OCH_2CH_2)_mOH$ and $\tilde{\varepsilon} \equiv (n - m)/(m + n)$ characterises the asymmetry of the amphiphile (see ref. 47 for details). Taking typical parameter values, $a = 10$ Å, $b = 15$ Å, $\Sigma = 70$ Å^2, $kT = 4 \times 10^{-21}$ J, from eqn. (6.7) one calculates $\lambda = 9.8 \times 10^6$ Pa, which is close to the values of λ estimated above. The dimensionless multiplier $(a_3b^3)/(2\Sigma^2)$ takes the value 1.06 and consequently eqn. (6.7) gives $k_c \approx kT$ for the small values of $\tilde{\varepsilon}$, *viz.*

$$\tilde{\varepsilon} = 0,\ 0.025,\ 0.1 \text{ and } -0.1 \quad (6.8)$$

used in ref. 47. We recall that we also used $k_c \approx kT$.

Concerning eqn. (6.6), we first note that the surface tension effect is not taken into account in ref. 47; in so far as the term, $\sigma_0(d\zeta/dx)^2$, is missing in eqn. (6.3). In other words, the model based on eqn. (6.3) is designed for flaccid membranes. [Correspondingly, non-monotonic curves for $\zeta(x)$ and $F_d(L)$ are obtained in ref. 47.] Therefore, it is correct to set $\sigma_0 = 0$ in eqn. (6.6) and to compare the bending moment terms:

$$B_0' \equiv \Sigma\frac{\partial B_0}{\partial\Sigma} = 4\left(\frac{\partial\kappa}{\partial\Sigma} - \frac{\kappa}{\Sigma}\right) \quad (6.9)$$

Then one finds a simple relation between the bending moments in the two models:

$$B_0 = \frac{4\kappa}{\Sigma} = -\frac{8a_2v^2\tilde{\varepsilon}kT}{\Sigma^4} \quad (6.10)$$

where at the last step we used the molecular model accepted in ref. 47, with $v = \Sigma_\infty b$ being the volume per amphiphile and Σ_∞ being the area per lipid in the non-disturbed bilayer. In addition, from eqn. (6.9) and (6.10) one may derive

$$B_0' = \frac{32a_2v^2\tilde{\varepsilon}kT}{\Sigma^4} \approx \frac{32a_2b^2\tilde{\varepsilon}kT}{\Sigma_\infty^2} \quad (6.11)$$

With the parameters values used above, including the values $\tilde{\varepsilon}$ given in eqn. (6.8), from eqn. (6.10) and (6.11) one may calculate

$$B_0 = (0,\ -0.11,\ -0.45 \text{ and } +0.45) \times 10^{-11} \text{ N} \quad (6.12)$$

$$B_0 = (0,\ 0.44,\ 1.8 \text{ and } -1.8) \times 10^{-11} \text{ N} \quad (6.13)$$

The latter values are to be compared with the values $B_0 = 7 \times 10^{-11}$ N and $B_0' = -3.2 \times 10^{-11}$ N used by us, which are calculated from the experimental Hamaker constants and ΔV potential, see Appendix A.

In summary, despite the quite different physical formulations of the two models, their parameters can be identified: see eqn. (6.2), (6.5), (6.9) and (6.10). An exception is the surface tension effect, which is disregarded in ref. 47 (σ_0 is set zero).

Concluding Remarks

The results of the present study can be summarised as follows:

(1) A 'sandwich model' of a lipid bilayer has been developed. The bilayer is modelled as an elastic layer (the hydrocarbon-chain zone) sandwiched between two Gibbs dividing surfaces representing the two lipid head-group regions, see Fig. 2 and 4. Expressions for the bilayer stretching, bending and torsion elasticities have been derived, see eqn. (1.19)–(1.21).

(2) To achieve an adequate description of the bilayer interior as a continuous medium, different constitutive relations (relating stress and strain) have been used with the different independent modes of bilayer deformation *viz.* constitutive relation of an isotropic incompressible elastic body, eqn. (2.2), for the stretching (Fig. 3) and bending (Fig. 13) modes and a hybrid constitutive relation, eqn. (2.4) for the squeezing mode (Fig. 5). The latter mode is related to the deformations around inclusions and to the lateral capillary forces between them (Fig. 6). In a more general case when the displacement vector can be expressed as a sum of components due to the various independent modes of deformation,

$$\boldsymbol{u} = \boldsymbol{u}_{\text{stretching}} + \boldsymbol{u}_{\text{bending}} + \boldsymbol{u}_{\text{squeezing}}$$

each component can be determined separately, by using the constitutive relation for the respective independent mode.

(3) Equations governing the bilayer profile have been derived, see eqn. (2.26) and (2.32). The bilayer shape has been determined in the presence of one and two cylindrical inclusions, see eqn. (3.3), (3.8)–(3.11) and Fig. 8. The calculations were carried out for not-too-flaccid bilayers [eqn. (2.30) holds], when the deformations decay monotonically far from the inclusions. However, it should be noted that eqn. (2.26) predicts oscillatory decaying deformations for flaccid bilayers.

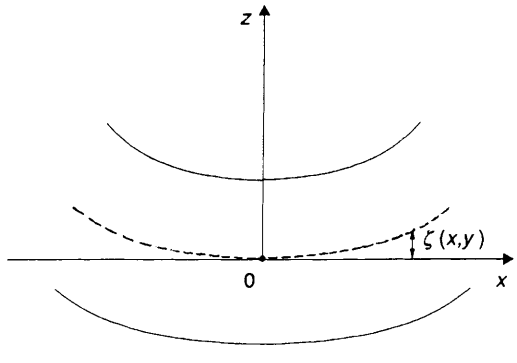

Fig. 13 Bending deformation of an initially planar lipid bilayer; $\zeta(x, y)$ represents the shape of the bilayer midsurface after the deformation

(4) Expressions for the lateral force, eqn. (5.17), and interaction energy, eqn. (5.22), were obtained. The calculated interaction energy $\Delta\Omega(L)$ can be of the order of several kT for not-too-small values of the mismatch h_c, see Fig. 10 and 11. The range of the interaction turns out to be of the order of several inclusion radii. In the case of concave menisci the interaction is stronger compared with the case of convex menisci for the same inclusions with the same $|h_c|$, Fig. 11; this result is in a qualitative agreement with experimental observations of Lewis and Engelman.[27]

(5) For calculating estimates, an asymptotic formula, eqn. (5.23) was derived, which compares well with the exact solution, Fig. 12.

(6) Our model was compared with the phenomenological model by Dan *et al.*[47] and relations between the parameters of the two models have been obtained, eqn. (6.2), (6.5), (6.9) and (6.10).

We hope that the detailed theoretical model developed in the present study will be helpful for interpretation of the processes of protein aggregation in lipid bilayers as well as for any processes affected by the membrane stretching and bending elastic properties.

This study was supported by the Research and Development Corporation of Japan (JRDC) under the Nagayama Protein Array Project of the Programme 'Exploratory Research for Advanced Technology' (ERATO). The authors are indebted to Miss Mariana Paraskova for typing the manuscript and drawing the figures.

Appendix A: Bending of Bilayers

Here we consider flexural deformations of a lipid bilayer under the condition for small deviations from planarity. In such a case the work of flexural deformation of the bilayer (membrane) is usually represented by means of the following phenomenological expression[61,78]

$$\Delta w_b = 2k_t H^2 + \bar{k}_t K \tag{A.1}$$

where H and K are the mean and the Gaussian curvatures;[69] the other notation is the same as in eqn. (1.20) and (1.21).

By means of our 'sandwich model' of a lipid bilayer we derive below an equation of the type of eqn. (A.1) and thus we obtain expressions determining the phenomenological parameters k_t and $\bar{k}_t$. In the framework of this model one can write

$$\Delta w_b = \Delta w_s + \Delta w_{in} \tag{A.2}$$

Here Δw_s and Δw_{in} are contributions due to the bilayer surfaces and the bilayer interior, which are considered separately below.

(*a*) Flexural Deformation of the Bilayer Interior

The initial state is a planar bilayer. Let the equation of the bilayer midsurface after the deformation be

$$z = \zeta(x, y) \tag{A.3}$$

(see Fig. 13). As a bilayer subjected to such a deformation cannot exhibit its two-dimensional fluidity, we will treat the chain region as an incompressible elastic medium. In other words eqn. (2.1) and (2.2) hold. Then in the same way as in ref. 59, eqn. (1.4), one derives

$$u_{xx} = -z\frac{\partial^2\zeta}{\partial x^2}; \qquad u_{yy} = -z\frac{\partial^2\zeta}{\partial y^2}; \qquad u_{xy} = -z\frac{\partial^2\zeta}{\partial x\partial y};$$

$$u_{xz} = u_{yz} = 0; \qquad u_{zz} = z\left(\frac{\partial^2\zeta}{\partial x^2} + \frac{\partial^2\zeta}{\partial y^2}\right) \tag{A.4}$$

Since the free energy per unit area is[59]

$$\Delta w_{in} = \frac{1}{2}\int_{-h/2}^{h/2} \tau_{ik}\, u_{ik}\, dz \tag{A.5}$$

the substitution of eqn. (2.2) and (A.4) in eqn. (A.5) after some transformations yields[59,79]

$$\Delta w_{in} = \frac{2}{3}\lambda h^3 H^2 - \frac{1}{6}\lambda h^3 K \tag{A.6}$$

We have used the fact that in linear approximation one can write[59]

$$2H = \frac{\partial^2\zeta}{\partial x^2} + \frac{\partial^2\zeta}{\partial y^2}; \qquad K = \frac{\partial^2\zeta}{\partial x^2}\frac{\partial^2\zeta}{\partial y^2} - \left(\frac{\partial^2\zeta}{\partial x\partial y}\right) \tag{A.7}$$

In addition, let us denote by

$$\alpha_1 = (u_{xx} + u_{yy})|_{z=-h/2}; \qquad \alpha_2 = (u_{xx} + u_{yy})|_{z=h/2};$$

$$\Delta h = \int_{-h/2}^{h/2} u_{zz}\, dz \tag{A.8}$$

the relative dilatation of the lower and upper bilayer surfaces and the change in the bilayer thickness. By means of eqn. (A.4) and (A.8) one obtains

$$\alpha_2 = -\alpha_1; \qquad \Delta h = 0 \tag{A.9}$$

i.e. the lower surface is extended, the upper surface is compressed and the film thickness does not change (in linear approximation) during the considered flexural deformation.

(*b*) Flexural Deformation of the Bilayer Surfaces

The work of interfacial deformation per unit area can be represented in the form[61,77,80]

$$dw = \gamma d\alpha + \xi d\beta + B dH + \Theta dD \tag{A.10}$$

where

$$\alpha = a^{\mu\nu}u_{\mu\nu}; \qquad \beta = q^{\mu\nu}u_{\mu\nu} \tag{A.11}$$

characterise the magnitude of surface dilatation and shear; $a^{\mu\nu}$ are components of the surface metric tensor,

$$q^{\mu\nu} = \frac{1}{D}(b^{\mu\nu} - Ha^{\mu\nu}) \tag{A.12}$$

is curvature deviatoric tensor[61,63,77]

$$H = \frac{1}{2}a^{\mu\nu}b_{\mu\nu} = \frac{1}{2}(c_1 + c_2); \qquad D = \frac{1}{2}q^{\mu\nu}b_{\mu\nu} = \frac{1}{2}(c_1 - c_2) \tag{A.13}$$

are the mean and the deviatoric curvatures, respectively, with c_1 and c_2 being the two principle curvatures of the interface. B and Θ are the surface bending and torsion moments. γ and ξ are the thermodynamical dilatational and shear tensions, which differ from the corresponding mechanical tensions, σ and η, entering the expression for the surface stress tensor:

$$\sigma_{\mu\nu} = \sigma a_{\mu\nu} + \eta q_{\mu\nu} \tag{A.14}$$

In general, it can be proven[61,80]

$$\gamma = \sigma + \frac{1}{2}BH + \frac{1}{2}\Theta D \tag{A.15}$$

$$\xi = \eta + \frac{1}{2} BD + \frac{1}{2} \Theta H \tag{A.16}$$

As mentioned earlier, the bilayer surfaces behave like a two-dimensional fluid; hence $\sigma_{\mu\nu}$ should be an isotropic tensor:

$$\eta = 0 \tag{A.17}$$

cf. eqn. (2.22) and (A.14). In keeping with eqn. (A.10) one can present the elementary work of deformation of the bilayer surfaces in the form

$$\mathrm{d}w_s = \sum_{k=1,2,} [\gamma_k \,\mathrm{d}\alpha_k + \xi_k \,\mathrm{d}\beta_k + B_k \,\mathrm{d}H_k + \Theta_k \,\mathrm{d}D_k] \tag{A.18}$$

where the indices 1 and 2 refer to the lower and upper bilayer surfaces, respectively. As before, we assume that the bilayer surfaces can be described as Helfrich interfaces for which[61]

$$B_k = B_0 + 2(2k_c + \bar{k}_c)H_k;$$
$$\Theta_k = -2\bar{k}_c D_k; \qquad k = 1, 2 \tag{A.19}$$

In fact, eqn. (A.19) gives the expansion of B_k and Θ_k for small curvature. B_0 is the bending moment of a flat bilayer surface; it is related to the so-called spontaneous curvature, H_0, by means of the expression[61] $B_0 = -4k_c H_0$; k_c and $\bar{k}_c$ are the bending and torsion elasticities of the bilayer surfaces. By using eqn. (A.4), (A.7), (A.8) and (A.11)–(A.13) in linear approximation one can derive

$$-H_1 = H_2 = H; \qquad -D_1 = D_2 = D \tag{A.20}$$

(H and D refer to the midsurface)

$$\alpha_k = -hH_k; \qquad \beta_k = -hD_k; \qquad k = 1, 2 \tag{A.21}$$

In general, the bending moment of an interfacial monolayer, B_0, depends on the relative dilation, α:

$$B_0(\alpha) = B_{00} + \left.\frac{\partial B_0}{\partial \alpha}\right|_{\alpha=0} \alpha + O(\alpha^2) \tag{A.22}$$

The last equation combined with eqn. (A.19) and (A.21) yields (in linear approximation)

$$B_k = B_{00} + (4k_c - 2\bar{k}_c - B'_0 h)H_k; \qquad B'_0 \equiv \left.\frac{\partial B_0}{\partial \alpha}\right|_{\alpha=0} \tag{A.23}$$

In addition, from eqn. (A.16), (A.17), (A.20) and the Gibbs–Duhem equation, $\mathrm{d}\gamma_k = E_G \,\mathrm{d}\alpha_k + \xi_k \,\mathrm{d}\beta_k + B_k \,\mathrm{d}H_k + \Theta_k \,\mathrm{d}D_k$, in linear approximation one derives

$$\gamma_k = \sigma_0 + E_G \alpha_k + B_0 H_k; \qquad \xi_k = \frac{1}{2} B_0 D_k; \qquad k = 1, 2 \tag{A.24}$$

On substituting eqn. (A.19)–(A.23) into eqn. (A.18) and integrating, one obtains the desired expression for Δw_s:

$$\Delta w_s = \left[E_G h^2 - \left(\frac{3}{2} B_{00} + B'_0\right)h + 4k_c\right]H^2 + \left(\frac{1}{2} B_0 h + 2\bar{k}_c\right)K \tag{A.25}$$

Finally, a combination of eqn. (A.1), (A.6) and (A.25) leads to eqn. (1.20) and (1.21).

The term $E_G h^2/2$ in eqn. (1.20) and (A.25) was first obtained by Evans and Skalak,[32] who derived $k_t = 1/2E_G h^2$ by means of model considerations. As demonstrated below the term proportional to h turns out to be comparable in magnitude with $E_G h^2$; this term gives a considerable contribution to k_t and dominates $\bar{k}_t$.

To estimate B_0 we first note that (by analogy with the DLVO theory of disjoining pressure) the bending moment of a flat interface can be represented as a sum of contributions due to the van der Waals and electrostatic (double layer) forces:[81]

$$B_0 = B_0^{vw} + B_0^{el} \tag{A.26}$$

Expressions for B_0^{vw} and B_0^{el} are available.[82,83]

$$B_0^{vw} = \frac{8}{5}(\Lambda_1 - \Lambda_2)\left(\frac{\gamma_0}{5\pi A_H}\right)^{1/5}; \qquad B_0^{el} = \frac{\varepsilon}{8\pi}(\Delta V)^2 \tag{A.27}$$

Here ΔV is the surface potential[84] of a dense lipid monolayer at an oil–water interface [ΔV in eqn. (A.27) must be substituted in CGSE-units, *i.e.* the value of ΔV in volts must be divided by 300]; ε is the relative permittivity. Since the headgroup region contains mainly water of hydration (incorporated in the hydration shells around the zwitterions), we take $\varepsilon = 32$, see *e.g.* ref. 84; $\gamma_0 \approx 50$ mN m^{-1} is the surface tension of a pure water–hydrocarbon interface; A_H, Λ_1 and Λ_2 are the compound and partial Hamaker constants:[82]

$$A_H = \Lambda_1 + \Lambda_2\Lambda_1 = \pi^2(\alpha_{11}\rho_1^2 - \alpha_{12}\rho_1\rho_2);$$
$$\Lambda_2 = \pi^2(\alpha_{22}\rho_2^2 - \alpha_{12}\rho_1\rho_2) \tag{A.28}$$

where ρ_1 and ρ_2 are the number densities of the oil and water phases and α_{ik} are the constants in the intermolecular van der Waals potential $u_{ik} = -\alpha_{ik}/r^6$. With typical parameters values one calculates[82] $B_0^{vw} \approx 5.3 \times 10^{-11}$ N. With the value $\Delta V \approx 350$ mV measured in ref. 85 and 86 with lipid monolayers one calculates $B_0^{el} = 1.7 \times 10^{-11}$ N. In view of eqn. (A.26) one obtains $B_{00} \approx 7 \times 10^{-11}$ N.

Assuming that the Hamaker constant in the region of the hydrated lipid headgroups is close to the Hamaker constant of water, one estimates $\partial B_0^{vw}/\partial\alpha \approx 0$. Then eqn. (A.26) and (A.27) imply

$$\frac{\partial B_0}{\partial \alpha} \approx \frac{\partial B_0^{el}}{\partial \alpha} = \frac{\varepsilon}{4\pi} \Delta V \frac{\partial \Delta V}{\partial \alpha} \tag{A.29}$$

There is plenty of experimental data for examining the ΔV *vs.* α dependence for dense lipid monolayers; thus from Fig. 3 in ref. 64 we calculate $\partial\Delta V/\partial\alpha = -323$ mV, and then with $\Delta V = 350$ mV and $\varepsilon = 32$, eqn. (A.19) yields

$$B'_0 \equiv \frac{\partial B_0}{\partial \alpha} = -3.2 \times 10^{-11} \text{ N} \tag{A.30}$$

with the above values of ε and ΔV. The values of B_{00} and B'_0 thus calculated characterise the phosphatidylcholine headgroups and do not depend on the length of the hydrocarbon chains, *cf.* ref. 64. For numerical estimates we use also other typical parameters values: $h = 3.6$ nm, $E_G = 40$ mN m^{-1}, $\lambda = 3 \times 10^6$ N m^{-2}, $k_c \approx \bar{k}_c \approx 4 \times 10^{-21}$ J. Then the values of the terms in eqn. (1.20) and (1.21) ($\times 10^{-19}$ J) are

$$2k_c = 0.08; \qquad -\left(\frac{3}{2} B_{00} + B'_0\right)\frac{h}{2} = -1.31;$$
$$\frac{1}{2} E_G h^2 = 2.59; \qquad \frac{1}{3}\lambda h = 0.47 \tag{A.31}$$
$$2\bar{k}_c = 0.08; \qquad \frac{1}{2} B_0 h = 1.26; \qquad -\frac{1}{6}\lambda h^3 = -0.23 \tag{A.32}$$

The substitution of eqn. (A.31) and (A.32) into eqn. (1.20) and (1.21) yields

$$k_t = 1.8 \times 10^{-19}\ \text{J}, \qquad \bar{k}_t = 1.1 \times 10^{-19}\ \text{J} \tag{A.33}$$

The latter value of k_t is close to the experimental values determined in ref. 37. Moreover, the chain elasticity contribution, *viz.* $\lambda h^3/3$, is *ca.* 25% of k_t, which is consonant with the discussion in ref. 37.

Appendix B: Derivation of eqn. (2.24) and (5.13)

The tensor of interfacial moments (torques) can be represented in the form[61,80]

$$M^{\mu\nu} = \frac{1}{2}(a^{\mu\nu}B + q^{\mu\nu}\Theta) \tag{B.1}$$

where $q^{\mu\nu}$ is defined by eqn. (A.12). The general thermodynamic definitions of the interfacial bending and torsion moments are[61,87]

$$B = \left(\frac{\partial w_f}{\partial H}\right)_{D,\alpha}; \qquad \Theta = \left(\frac{\partial w_f}{\partial D}\right)_{H,\alpha} \tag{B.2}$$

where w_f is the work of flexural deformation per unit area of the interface. To obtain an explicit relation between $M^{\mu\nu}$ and the surface curvatures one needs an appropriate constitutive relation. The latter is provided by the Helfrich formula[78]

$$w_f = 2k_c(H - H_0)^2 + \bar{k}_c K \tag{B.3}$$

where k_c, $\bar{k}_c$ and H_0 are constants with respect to the curvatures. Combining eqn. (B.1)–(B.3) one derives[61]

$$M^{\mu\nu} = [(2k_c + \bar{k}_c)H + B_0/2]a^{\mu\nu} - \bar{k}_c D q^{\mu\nu} \tag{B.4}$$

where $B_0 \equiv -4k_c H_0$. Further, by using eqn. (1.12), (2.3), (2.8) and (2.9) one obtains

$$\alpha = -2\zeta/h \tag{B.5}$$

for the specified type of deformation. Eqn. (A.12), (A.22), (B.4) and (B.5), along with the identity $b^{\mu}_{\cdot\nu} = 2H^{\cdot\mu}$, lead to the eqn. (2.24). Note that eqn. (2.24) holds in linear approximation for small deviations from planarity; quadratic and higher-order terms are neglected.

Next we proceed with the derivation of eqn. (5.13). First we note that the vectors of a covariant local basis in the upper bilayer surface can be expressed in the form[66]

$$\boldsymbol{a}_\nu = \boldsymbol{e}_\nu + \boldsymbol{e}_z \zeta_{,\nu}; \qquad \nu = 1, 2 \tag{B.6}$$

where the vectors $\boldsymbol{e}_1$ and $\boldsymbol{e}_2$ form a basis in the plane xy. Then by using eqn. (2.4), (2.8), (2.13), (2.16) and (B.6) one can transform the last term in eqn. (2.20) to read

$$\boldsymbol{n} \cdot \boldsymbol{\tau} \cdot \boldsymbol{a}_\nu = 2(2\lambda/h)\zeta\zeta_{,\nu}(1 + |\nabla_\Pi \zeta|^2)^{-1/2} \tag{B.7}$$

On substituting eqn. (2.22), (2.23), (5.2) and (B.7) into eqn. (2.20) one derives

$$\nabla_\Pi \sigma + (k_c q^2 - B_0'/h)\boldsymbol{b} \cdot \nabla_\Pi \zeta = (P_T - P_0)\nabla_\Pi \zeta + (2\lambda/h - \Pi')\nabla_\Pi \zeta^2 \tag{B.8}$$

where higher-order terms are neglected. Moreover, in linear approximation one can write

$$\boldsymbol{b} \cdot \nabla_\Pi \zeta = (\nabla_\Pi \nabla_\Pi \zeta) \cdot \nabla_\Pi \zeta = \frac{1}{2}\nabla_\Pi |\nabla_\Pi \zeta|^2 \tag{B.9}$$

On substituting eqn. (B.9) into eqn. (B.8) and integrating one finally derives eqn. (5.13). The constant of integration is obviously the surface tension σ_0 of the non-disturbed plane-parallel bilayer of thickness h.

Appendix C: Expression for the Grand Thermodynamic Potential

Following an heuristic approach we present the bilayers grand thermodynamic potential down as the grand potential of a thin liquid film of surface tension σ and reference pressure P_T (*cf.* ref. 51):

$$\Omega = 2\int_S \mathrm{d}s\sigma - \int_{V_{in}} \mathrm{d}V P_T - \int_{V_{out}} \mathrm{d}V P_0 \tag{C.1}$$

where S symbolises the bilayer surface, and V_{in} and V_{out} denote, respectively, the volume of the bilayer interior and the outer aqueous phase. The effect of hydrocarbon chain elasticity and the curvature effects are contained implicitly in σ. Indeed, by using eqn. (5.13) one obtains

$$\int_S \mathrm{d}s\sigma = \int_{S_0} \mathrm{d}s\sqrt{(1 + |\nabla_\Pi \zeta|^2)}[\sigma_0 - \frac{1}{2}(k_c q^2 - B_0'/h)|\nabla_\Pi \zeta|^2 + (P_T - P_0)\zeta + (2\lambda/h - \Pi')\zeta^2]$$

where the meaning of S_0 is the same as in eqn. (5.19). In addition,

$$\int_{V_{in}} \mathrm{d}V P_T + \int_{V_{out}} P_0 = 2\int_{S_0} \mathrm{d}s\left[\int_0^{b+\zeta} \mathrm{d}z P_T + \int_{b+\zeta}^{z_1} \mathrm{d}z P_0\right]; \qquad b = h/2$$

where the exact position of the plane $z = z_1$ is not important since it does not affect the final result. Now one can easily derive eqn. (5.19) from eqn. (C.1).

The validity of eqn. (5.19) can be verified by checking the correctness of its predictions. Thus by using variations at fixed boundaries from eqn. (5.19) one derives

$$\tilde{\sigma}_0 \nabla_\Pi^2 \zeta - k_c q^2 \nabla_\Pi^2 \nabla_\Pi^2 \zeta = 2(2\lambda/h - \Pi')\zeta \tag{C.2}$$

which is equivalent to eqn. (2.26) in view of eqn. (2.32). Moreover, by using variations at movable boundaries one can derive

$$\frac{\delta\Omega}{\delta t} = -F_x \tag{C.3}$$

where F_x and Ω are defined by eqn. (5.17) and (5.19), respectively; the proof is as follows.

Let C_1 and C_2 be the contours in the plane xy cut by the left- and right-hand side inclusion, respectively (Fig. 7). Let us translate the right-hand side inclusion at a distance δL along the x-axis, while the position of the left-hand side inclusion remains fixed. Correspondingly, the contour C_2 transforms into C_2', whereas the contour C_1 remains fixed. This variation causes a change in the bilayer profile $\zeta(x, y)$ with $\delta\zeta(x, y)$. Let us denote

$$\delta\zeta_1 = \delta\zeta(x, y) \text{ for } (x, y) \in C_1; \qquad \delta\zeta_2 = \delta\zeta(x, y) \text{ for } (x, y) \in C_2' \tag{C.4}$$

In addition, one can write[88]

$$\delta\zeta_1 = \delta\zeta|_{C_1}; \qquad \delta\zeta_2 = \delta\zeta|_{C_2} + \delta\boldsymbol{r} \cdot (\nabla_\Pi \zeta)|_{C_2} \tag{C.5}$$

where $\delta\boldsymbol{r}$ is the vector of displacement of contour C_2. In our case $\delta\boldsymbol{r} = (\delta L, 0)$. In so far as we deal with fixed positions of the contact lines at the inclusion surfaces, we can write

$$\delta\zeta_1 = \delta\zeta_2 = 0 \tag{C.6}$$

Besides, we express the equation of contour C_2 in the form

$$x = x(l); \qquad y = y(l) \tag{C.7}$$

where l is the natural parameter of length along C_2. Then, in the same way as in ref. 51, one can prove that the variation

$\delta\Omega$, corresponding to the variation δL, can be presented in the form

$$\delta\Omega = \int_{S_0} \mathrm{d}s\delta\Phi - \oint_{C_2} \mathrm{d}l \frac{\mathrm{d}y}{\mathrm{d}l} \Phi\delta L \tag{C.8}$$

where

$$\Phi = (\tilde{\sigma}_0 - k_c q^2)|\nabla_{II}\zeta|^2 + 2(\lambda/h - \Pi')\zeta^2 \tag{C.9}$$

is the integrand of eqn. (5.19). Further, one can derive

$$\delta\Phi = 2[-(\tilde{\sigma}_0 - k_c q^2)\nabla_{II}^2\zeta + 2(2\lambda/h - \Pi')\zeta]\delta\zeta + 2(\tilde{\sigma}_0 - k_c q^2)\nabla_{II} \cdot [(\nabla_{II}\zeta)\delta\zeta] \tag{C.10}$$

By using eqn. (C.5)–(C.10) and Green's integral theorem, one obtains

$$\frac{\delta\Omega}{\delta L} = (\tilde{\sigma}_0 - k_c q^2) \oint_{C_2} \mathrm{d}l \left\{ 2\left[(\boldsymbol{m} \cdot \nabla_{II}\zeta) \frac{\partial\zeta}{\partial x} - \frac{\mathrm{d}y}{\mathrm{d}l} |\nabla_{II}\zeta|^2 \right] + \frac{\mathrm{d}y}{\mathrm{d}l} |\nabla_{II}\zeta|^2 \right\} \tag{C.11}$$

As usual, $\boldsymbol{m}$ is the unit tangent to C_2, which can be expressed as follows

$$\boldsymbol{m} = \boldsymbol{e}_x \cos\phi - \boldsymbol{e}_y \sin\phi = \frac{\mathrm{d}y}{\mathrm{d}l}\boldsymbol{e}_x - \frac{\mathrm{d}x}{\mathrm{d}l}\boldsymbol{e}_y \tag{C.12}$$

With the help of eqn. (C.12) one derives

$$-(\boldsymbol{m} \cdot \nabla_{II}\zeta) \frac{\partial\zeta}{\partial x} + \frac{\mathrm{d}y}{\mathrm{d}l} |\nabla_{II}\zeta|^2 = \left(\frac{\partial\zeta}{\partial x}\frac{\mathrm{d}x}{\mathrm{d}l} + \frac{\partial\zeta}{\partial y}\frac{\mathrm{d}y}{\mathrm{d}l} \right) \frac{\partial\zeta}{\partial y} = \frac{\mathrm{d}\zeta}{\mathrm{d}l}\frac{\partial\zeta}{\partial y} = 0$$

Note that $\mathrm{d}\zeta/\mathrm{d}l = 0$ because the contact line is horizontal. Then eqn. (C.11) reduces to

$$\frac{\delta\Omega}{\delta L} = (\tilde{\sigma}_0 - k_c q^2) \oint_{C_2} \mathrm{d}l |\nabla_{II}\zeta|^2 \cos\phi = -F_x$$

which was to be proven. At the last step we utilised eqn. (5.16), (5.17) and (C.12).

Appendix D: Asymptotic Formula for the Interaction Energy

Here we seek the solution of eqn. (2.32) which satisfies the boundary condition

$$\zeta|_{C_1} = \zeta|_{C_2} = h_c \tag{D.1}$$

where C_1 and C_2 symbolise the contact lines of the two inclusions, Fig. 7. We will make use of the method of reflections, which was introduced by Smoluchowski in 1911 and extended to various hydrodynamic problems by Happel and Brenner.[89] Following this method we take as a zeroth-order approximation the solution for a single inclusion, *cf.* eqn. (3.3):

$$\zeta_1^{(0)} = A_0 K_0(q|\boldsymbol{r}|); \qquad \zeta_2^{(0)} = A_0 K_0(|\boldsymbol{r} - \boldsymbol{L}|) \tag{D.2}$$

$A_0 = h_c/K_0(qr_c)$; the coordinate origin is chosen to be the intersection point of the axis of the left-hand side inclusion with the plane xy; $L = |\boldsymbol{L}|$; the subscripts 1 and 2 symbolise the left- and right-hand side inclusion, respectively. Then the simple superposition approximation yields

$$\zeta = \zeta_1^{(0)} + \zeta_2^{(0)} \tag{D.3}$$

One can check that $\zeta_1^{(0)}$ satisfies the boundary condition at C_1, and $\zeta_2^{(0)}$ the conditions at C_2, but ζ as given by eqn. (D.3) does not satisfy the boundary condition either at C_1 or at C_2. The aim of the method of reflections is to remove this drawback. This is achieved by using a series of correction terms, each of them satisfying eqn. (2.32) with appropriate boundary conditions. The first correction term is

$$\zeta_2^{(1)}(\boldsymbol{r}) = -A_1 K_0(q|\boldsymbol{r}|), \tag{D.4}$$

which is to satisfy the boundary condition

$$\zeta_1^{(1)}|_{C_1} = -\zeta_2^{(0)}|_{C_1} \approx -A_0 K_0(qL); \qquad r_c \ll L \tag{D.5}$$

One sees that $\zeta_1^{(1)}$ is intended to remove the violation of the boundary condition at C_1 introduced by $\zeta_2^{(0)}$ in eqn. (D.3). From eqn. (D.4) and (D.5) one determines

$$A_1 = A_0 K_0(qL)/K_0(qr_c) \tag{D.6}$$

A symmetric correction at C_2 is provided by the function

$$\zeta_2^{(1)}(\boldsymbol{r}) = -A_1 K_0(q|\boldsymbol{r} - \boldsymbol{L}|) \tag{D.7}$$

The next-order corrections, satisfying the boundary condition

$$\zeta_i^{(2)}|_{C_i} = -\zeta_j^{(1)}|_{C_i} \approx -[A_0 K_0(qL)]; \qquad i, j = 1, 2; \qquad i \neq j \tag{D.8}$$

and

$$\zeta_1^{(2)}(\boldsymbol{r}) = A_2 K_0(q|\boldsymbol{r}|); \qquad \zeta_2^{(2)}(\boldsymbol{r}) = A_2 K_0(q|\boldsymbol{r} - \boldsymbol{L}|) \tag{D.9}$$

with

$$A_2 = A_1 K_0(qL)/K_0(qr_c) \tag{D.10}$$

The procedure can be continued in a similar way; thus one obtains

$$\zeta_1^{(j)}(\boldsymbol{r}) = A_j K_0(q|\boldsymbol{r}|); \qquad \zeta_2^{(j)}(\boldsymbol{r}) = A_j K_0(q|\boldsymbol{r} - \boldsymbol{L}|) \tag{D.11}$$

with

$$A_j = A_{j-1} K_0(qL)/K_0(qr_c); \qquad j = 1, 2, 3, \ldots \tag{D.12}$$

Then the method of reflections[89] provides the following generalisation of eqn. (D.3):

$$\zeta(\boldsymbol{r}) = \sum_{j=0}^{\infty} [\zeta_1^{(j)}(\boldsymbol{r}) + \zeta_2^{(j)}(\boldsymbol{r})] \tag{D.13}$$

On substituting eqn. (D.11) and (D.12) into eqn. (D.13) and summing over the resulting series one derives

$$\zeta(\boldsymbol{r}) = h_c \frac{K_0(q|\boldsymbol{r}|) + K_0(q|\boldsymbol{r} - \boldsymbol{L}|)}{K_0(qr_c) + K_0(qL)} \tag{D.14}$$

With the above expression for $\zeta(\boldsymbol{r})$ we next determine $\tan\Psi_c(L)$ from eqn. (5.21), which can be transformed to read

$$\tan\Psi_c(L) = -\frac{1}{2\pi}\int_0^{2\pi} \mathrm{d}\phi \left(\frac{\partial\zeta}{\partial r}\right)_{r=r_c} \tag{D.15}$$

In keeping with eqn. (D.14) one obtains

$$\left(\frac{\partial\zeta}{\partial r}\right)_{r=r_c} = \frac{-qh_c}{K_0(qr_c) + K_0(qL)} \times \left[K_1(qr_c) + K_1(qr_2)\left(\frac{\mathrm{d}r_2}{\mathrm{d}r}\right)_{r=r_c} \right]$$

where

$$r_2 \equiv |\boldsymbol{r} - \boldsymbol{L}| = (L^2 + r^2 - 2Lr\cos\phi)^{1/2} \tag{D.16}$$

Further we calculate $\mathrm{d}r_2/\mathrm{d}r$ at $r = r_c$ and expand the result in series, keeping the linear term with respect to r_c/L. Then from

eqn. (D.15) we calculate

$$\tan \Psi_c(L) \approx qh_c \frac{K_1(qr_c) - \frac{1}{2}qr_c K_0(qL)}{K_0(qr_c) + K_0(qL)} \qquad \text{(D.17)}$$

The substitution of eqn. (3.6) and (D.17) into eqn. (5.22) yields eqn. (5.23).

List of Notation

a parameter of the bipolar coordinates, eqn. (4.4)
$a_{\mu\nu}$ surface metric tensor
$\boldsymbol{a}_\mu$ vector of the local surface basis
A_H Hamaker constant
b half of the non-disturbed bilayer thickness
$b_{\mu\nu}$ surface curvature tensor
B interfacial bending moment
B_0 bending moment of flat interface
D deviatoric curvature, eqn. (A.13)
$\boldsymbol{e}_x, \boldsymbol{e}_y$ unit vectors of the axes in the xy plane
E_G Gibbs elasticity of a lipid monolayer
$\boldsymbol{F}$ lateral inclusion–inclusion force
h thickness of the bilayer hydrocarbon-chain zone
h_c meniscus elevation at the contact line, Fig. 6
H mean curvature
k Boltzmann constant
k_c bending elasticity of the bilayer surface
$\bar{k}_c$ torsion elasticity of the bilayer surface
k_t bending elasticity of the bilayer as a whole
$\bar{k}_t$ torsion elasticity of the bilayer as a whole
K Gaussian curvature
K_d bending elastic modulus of Dan *et al.*,[47] eqn. (6.2)
K_e bulk compressibility modulus
K_s bilayer stretching elastic modulus, eqn. (1.18)
K_0, K_1 modified Bessel functions of the zeroth and first order
l_0 width of the inclusion (protein) hydrophobic belt
L axis-to-axis distance between two inclusions
$\boldsymbol{m}$ unit normal to the lateral inclusion surface, Fig. 6
$M^{\mu\nu}$ Tensor of the surface moments (torques)
$\boldsymbol{n}$ unit normal to the inclusion surface
P_N, P_T components of the pressure tensor
q reverse capillary length, eqn. (2.31)
$q_{\mu\nu}$ deviatoric curvature tensor
r_c radius of a contact line
T temperature
$\boldsymbol{T}_I, \boldsymbol{T}_{II}$ stress tensor inside and outside the bilayer
$\boldsymbol{u}$ displacement vector
u_{ik} strain tensor
$\boldsymbol{U}$ spatial unit tensor
$\boldsymbol{U}_{II}$ unit tensor in the plane xy
ΔV surface potential
w_b work of flexural deformation per unit area
α relative dilatation, eqn. (1.12)
β relative shear, eqn. (A.11)
γ thermodynamic surface tension
γ_b bilayer tension
δ_{ij} Kroneker symbol
ε relative permittivity
ζ perturbation in bilayer thickness, Fig. 6
η mechanical surface shear tension
Θ interfacial torsion moment, eqn. (A.10)
κ bending moment in the model by Dan *et al.*[47]
λ bulk shear elasticity in the hydrocarbon-chain zone
ν unit tangent to the bilayer surface, Fig. 6
ξ thermodynamic surface shear tension, eqn. (A.10)
Π disjoining pressure
σ mechanical surface tension
σ_0 surface tension of the non-disturbed bilayer
Σ area per lipid molecule
τ bipolar coordinate, Fig. 7
τ_{ik} stress tensor component
ϕ azimuthal angle, eqn. (5.12)
Ψ_c (average) meniscus slope angle, eqn. (5.21), Fig. 6, 7
ω bipolar coordinate, Fig. 7
Ω grand thermodynamic potential

References

1 R. Henderson and P. N. T. Unwin, *Nature (London)*, 1975, **257**, 28.
2 R. Henderson, J. M. Baldwin, T. A. Ceska, F. Zemlin, E. Beckmann and K. H. Downing, *J. Mol. Biol.*, 1990, **213**, 899.
3 P. N. T. Unwin and G. Zampighi, *Nature (London)*, 1980, **283**, 545.
4 J. D. Robertson, *J. Cell. Biol.*, 1963, **19**, 201.
5 A. K. Mitra, M. P. McCarthy and R. M. Stroud, *J. Cell. Biol.*, 1989, **109**, 755.
6 A. Baroin, A. Bienvenue and P. F. Devaux, *Biochem.*, 1979, **18**, 1151.
7 J. N. Israelachvili, S. Marcelja and R. G. Horn, *Quart. Rev. Biophys.*, 1980, **13**, 121.
8 G. Benga and R. P. Holmes, *Prog. Biophys. Molec. Biol.*, 1984, **43**, 195.
9 E. Sackmann, R. Kotulla and F. J. Heiszler, *Can. J. Biochem. Cell Biol.*, 1984, **62**, 778.
10 S. Marcelja, *Biochim. Biophys. Acta*, 1976, **455**, 1.
11 H. Schröder, *J. Chem. Phys.*, 1977, **67**, 1617.
12 J. N. Israelachvili, *Biochim. Biophys. Acta*, 1977, **469**, 221.
13 M. Bloom, E. Evans and O. G. Mouritsen, *Quart. Rev. Biophys.*, 1991, **24**, 293.
14 P. Jost, O. H. Grifith, R. A. Capaldi and G. Vanderkooi, *Biochim. Biophys. Acta*, 1973, **311**, 141.
15 E. Favre, A. Baroin, A. Bienvenue and P. F. Devaux, *Biochem.*, 1979, **18**, 1156.
16 J. Davoust, A. Bienvenue, P. Fellmaqnn and P. F. Devaux, *Biochim. Biophys. Acta*, 1980, **596**, 28.
17 A. Bienvenue, M. Bloom, J. H. Davis and P. F. Devaux, *J. Biol. Chem.*, 1982, **257**, 3032.
18 J. H. Davis, D. M. Clare, R. S. Hodges and M. Bloom, *Biochem.*, 1983, **22**, 5298.
19 J. C. Huschilt, R. S. Hodges and J. H. Davis, *Biochem.*, 1985, **24**, 1377.
20 M. Esmann, A. Watts and D. Marsh, *Biochem.*, 1985, **24**, 1386.
21 R. D. Pates and D. Marsh, *Biochem.*, 1987, **26**, 29.
22 J. C. Owicki, M. W. Springgate and H. M. McConnell, *Proc. Natl. Acad. Sci. USA*, 1978, **75**, 1616.
23 J. C. Owicki and H. M. McConnell, *Proc. Natl. Acad. Sci. USA*, 1979, **76**, 4750.
24 C. Tanford, *The Hydrophobic Effect*, Wiley, New York, 1973.
25 J. N. Israelachvili, D. J. Mitchel and B. Ninham, *Biochim. Biophys. Acta*, 1977, **470**, 185.
26 Y. S. Chen and W. L. Hubbel, *Exp. Eye Res.*, 1973, **17**, 517.
27 B. A. Lewis and D. M. Engelman, *J. Mol. Biol.*, 1983, **166**, 203.
28 J. Riegler and H. Möhwald, *Biophys. J.*, 1986, **49**, 1111.
29 J. Peschke, J. Riegler and H. Möhwald, *Eur. Biophys. J.*, 1987, **14**, 385.
30 O. G. Mouritsen and M. Bloom, *Biophys. J.*, 1984, **46**, 141.
31 M. M. Sperotto and O. G. Mouritsen, *Eur. Biophys. J.*, 1991, **19**, 157.
32 E. Evans and R. Skalak, *CRC Crit. Rev. Bioeng.*, 1979, **3**, 181.
33 R. Kwok and E. Evans, *Biophys. J.*, 1981, **35**, 637.
34 D. Needham and R. Nunn, *Biophys. J.*, 1990, **58**, 997.
35 E. Evans and W. Rawicz, *Phys. Rev. Lett.*, 1990, **64**, 2094.
36 C. R. Safinya, E. B. Sirota, D. Roux and G. S. Smith, *Phys. Rev. Lett.*, 1989, **62**, 1134.
37 L. Fernandez-Puente, I. Bivas, M. D. Mitov and P. Méléard, *Europhys. Lett.*, 1994, **28**, 181.
38 A. G. Petrov and I. Bivas, *Prog. Surface Sci.*, 1984, **16**, 389.
39 I. Szleifer, D. Kramer, A. Ben-Shaul, W. M. Gelbart and S. A. Safran, *J. Chem. Phys.*, 1990, **92**, 6800.
40 M. Kléman, *Proc. R. Soc. London, A*, 1976, **347**, 387.
41 A. G. Petrov, M. D. Mitov and A. Derzhanski, in *Advances in Liquid Crystal Research and Applications*, Pergamon, Oxford, Academia Kiado, Budapest, 1980, p. 695.

42 S. Marcelja, *Biochim. Biophys. Acta*, 1974, **367**, 165.
43 D. W. R. Gruen, *Biochim. Biophys. Acta*, 1980, **595**, 161.
44 A. Ben-Shaul and W. M. Gelbart, *Ann. Rev. Phys. Chem.*, 1985, **36**, 179.
45 P. Helfrich and W. Jakobsson, *Biophys. J.*, 1990, **57**, 1075.
46 H. W. Huang, *Biophys. J.*, 1986, **50**, 1061.
47 N. Dan, P. Pincus and A. Safran, *Langmuir*, 1993, **9**, 2768.
48 P. A. Kralchevsky, V. N. Paunov, I. B. Ivanov and K. Nagayama, *J. Colloid Interface Sci.*, 1992, **151**, 79.
49 P. A. Kralchevsky, V. N. Paunov, N. D. Denkov, I. B. Ivanov and K. Nagayama, *J. Colloid Interface Sci.*, 1993, **155**, 420.
50 V. N. Paunov, P. A. Kralchevsky, N. D. Denkov, I. B. Ivanov and K. Nagayama, *J. Colloid Interface Sci.*, 1993, **157**, 100.
51 P. A. Kralchevsky and K. Nagayama, *Langmuir*, 1994, **10**, 23.
52 J. G. H. Joosten, in *Thin Liquid Films*, ed. I. B. Ivanov, M. Dekker, New York, 1988, p. 569.
53 C. Maldarelli, R. K. Jain, I. B. Ivanov and E. Ruckenstein, *J. Colloid Interface Sci.*, 1980, **78**, 118.
54 M. Goulian, R. Bruinsma and P. Pincus, *Europhys. Lett.*, 1993, **22**, 145.
55 S. J. Bussell, D. L. Koch and D. A. Hammer, *J. Fluid Mech.*, 1992, **243**, 679.
56 B. V. Derjaguin and E. V. Obuhov, *Nature* (*London*), 1936, **138**, 330.
57 J. N. Israelachvili, *Intermolecular and Surface Forces*, Academic Press, New York, 2nd ed., 1992.
58 B. V. Derjaguin, N. V. Churaev and V. M. Muller, *Surface Forces*, Plenum Press, New York, 1987.
59 L. D. Landau and E. M. Lifshitz, *Theory of Elasticity*, Pergamon Press, Oxford, 1970.
60 S. Ono and S. Kondo, in *Handbuch der Physik*, ed. S. Flügge, Springer, Berlin, 1960, vol. X.
61 P. A. Kralchevsky, J. C. Eriksson and S. Ljunggren, *Adv. Colloid Interface Sci.*, 1994, **48**, 19.
62 I. B. Ivanov and P. A. Kralchevsky, in ref. 52, p. 49.
63 A. I. Rusanov, *Phase Equilibrium and Surface Phenomena*, Khimia, Leningrad, 1967 (in Russian); *Phasengleichgewichte und Grenzflachenerscheinungen*, Akademie Verlag, Berlin, 1978.
64 J. Mingins, D. Stigter and K. A. Dill, *Biophys. J.*, 1992, **61**, 1603.
65 B. Y. Yue, C. M. Jackson, J. A. G. Taylor, J. Mingins and B. A. Pethica, *J. Chem. Soc., Faraday Trans. 1*, 1976, **72**, 2685.
66 P. A. Kralchevsky and I. B. Ivanov, *J. Colloid Interface Sci.*, 1990, **137**, 234.
67 P. M. Naghdi, in *Handbuch der Physik*, Springer, Berlin, 1972, vol. VIa/2.
68 Y. S. Podstrigach and Y. Z. Povstenko, *Introduction in Mechanics of Surface Phenomena in Deformable Solids*, Naukova Dumka, Kiev, 1985 (in Russian).
69 A. J. McConnell, *Application of Tensor Analysis*, Dover, New York, 1957.
70 L. D. Landau and E. M. Lifshitz, *Fluid Mechanics*, Pergamon Press, Oxford, 1984.
71 J. Meunier and L. T. Lee, *Langmuir*, 1991, **7**, 1855.
72 M. Abramowitz and I. A. Stegun, *Handbook of Mathematical Functions*, Dover, New York, 1965.
73 G. A. Korn and T. M. Korn, *Mathematical Handbook*, McGraw-Hill, New York, 1968.
74 A. Constantinides, *Applied Numerical Methods with Personal Computers*, McGraw-Hill, New York, 1987.
75 R. W. Hockney and J. W. Eastwood, *Computer Simulation Using Particles*, McGraw-Hill, New York, 1981.
76 P. N. T. Unwin and R. Henderson, *J. Mol. Biol.*, 1975, **94**, 425.
77 P. A. Kralchevsky, *J. Colloid Interface Sci.*, 1990, **137**, 217.
78 W. Helfrich, *Z. Naturforsch, C: Biosci.*, 1974, **29**, 1974.
79 A. E. H. Love, *A Treatise of the Mathematical Theory of Elasticity*, University Press, Cambridge, 1927.
80 T. D. Gurkov and P. A. Kralchevsky, *Colloids Surfaces*, 1990, **47**, 45.
81 P. A. Kralchevsky, T. D. Gurkov and I. B. Ivanov, *Colloids Surfaces*, 1991, **56**, 149.
82 T. D. Gurkov, P. A. Kralchevsky and I. B. Ivanov, *Colloids Surfaces*, 1991, **56**, 119.
83 P. A. Kralchevsky, T. D. Gurkov and K. Nagayama, *J. Colloid Interface Sci.*, 1995, submitted.
84 A. W. Adamson, *Physical Chemistry of Surfaces*, Wiley, New York, 1976.
85 R. C. McDonald and S. A. Simon, *Proc. Natl. Acad. Sci. USA*, 1987, **84**, 4089.
86 S. A. Simon, T. J. McIntosh and A. D. Magid, *J. Colloid Interface Sci.*, 1988, **126**, 74.
87 S. Ljuggren, J. C. Eriksson and P. A. Kralchevsky, *J. Colloid Interface Sci.*, 1993, **161**, 133.
88 L. E. Elsgoltz, *Differential Equations and Variational Calculus*, Nauka, Moscow, 1969 (in Russian).
89 J. Happel and H. Brenner, *Low Reynolds Number Hydrodynamics*, Prentice-Hall, New York, 1965; Martinus Nijhoff, The Hague, 1983.

Paper 5/02134K; *Received* 4*th April*, 1995